Numerical Weather Prediction

HadGEM1 Physics for the Global NWP Model (Cycle G34): Improvements to Boundary Layer, Large Scale Precipitation, Convection and Saharan Albedo.

Forecasting Research Technical Report No. 458

S.F. Milton, M. Brooks, A. Lock, E. Whelan, D. Wilson, R. Allan.

email:nwp˙publications@metoffice.gov.uk

Forecasting Research Technical Report No. 458

HadGEM1 Physics for the Global NWP Model (Cycle G34): Improvements to Boundary Layer, Large Scale Precipitation, Convection and Saharan Albedo.

Sean Milton, Malcolm Brooks, Adrian Lock, Eoin Whelan, and Damian Wilson
NWP, Met Office

Richard Allan,
ESSC*, The University of Reading.

16 March 2005

Abstract

Revisions to the boundary layer parametrization and large-scale precipitation scheme microphysics have been tested in the global NWP model along with a change to increase the Saharan albedo and some corrections/revisions to the convection scheme. Most of these changes are part of the physics package tested and successfully implemented in the new climate version of the Unified Model, HadGEM1. The boundary layer (BL) changes are mainly improvements to the diagnosis of mixed layer depths in the decoupled stratocumulus regime and the main change to the convection scheme is a reduction of the CAPE closure adjustment timescale from 1 hour to 30 minutes (not currently in HadGEM1). The main impacts from these two changes are in the tropics. There is reduced oceanic tropical precipitation and an increase in precipitation over tropical land masses, both of which correct known systematic errors in tropical precipitation. The changes in precipitation are accompanied by improvements in the tropical large-scale circulation. The 8B BL scheme also reduces low cloud over subtropical oceans which improves the radiation balance in comparisons with ERBE and GERB (Meteosat 8). The changes to the microphysics scheme are numerous, but one of the biggest physical impacts comes from increased autoconversion of liquid water to precipitation. This helps dissipate excessive low cloud in the model with improvements in near surface temperatures . A particular beneficial impact is seen on low cloud over Iraq. Finally, comparisons with ERBE and GERB top of the atmosphere clear sky radiation budgets suggest that Saharan surface albedo is underestimated, leading to excessive sensible heating of the surface. A change is made to increase Saharan albedo via the soil parameters which gives an improvement to the radiation budget and reduces circulation errors over the region.

1 Introduction.

Following the introduction of the new dynamical core (Davies *et al* (2005)) and revised (HADAM4) physics package in August 2002 (cycle G27), further developments were made to the physical parametrizations. These have been tested and implemented in the final release of the new climate version of the Unified Model (HadGEM1[1]). A number of these revisions have been tested in the global NWP model

*Environmental Systems Science Centre.

[1]Hadley Centre Global Environmental Model.

including (i) changes to the decoupled stratocumulus boundary layer (BL) types (8B BL scheme), (ii) revisions to the microphysics of large-scale precipitation (3C scheme), (iii) changes to the definition of surface albedo over the Sahara, and (iv) convection - a change of CAPE closure adjustment timescale from 1 hour to 30 minutes, and corrections to coding errors. This paper describes the impact of these changes on the global NWP model. Section 2 describes the changes and section 3 describes the tests carried out. Section 4 outlines results from a series of case studies run from operational analyses. In section 5 we consider results of the full package in offline trials with data assimilation and in a parallel trial. A summary and conclusions are given in section 6.

2 Model changes - HadGEM1 physics components.

This section describes the changes to model parametrization of BL turbulent mixing, large-scale precipitation, and Saharan albedo that form part of the HadGEM1 physics. Inclusion of these changes into the global NWP model will bring it in close agreement with the HadGEM1 formulation. An additional change to the convection parametrization to reduce the CAPE adjustment timescale from 1 hour to 30 minutes are also discussed. This is not currently part of HadGEM1.

a Changes to Boundary layer non-local mixing (version 8B BL).

The unstable BL scheme is described in detail in Lock *et al* (2000) and Martin *et al* (2000). The full mathematical details of the changes comprising the 8B BL scheme are given in Lock (2003b). The 8A BL formulation operational prior to January 2005 is described in Lock (2003a). A summary of the changes is given below.

a.1 *Revisions to depths of non-local mixing in decoupled Sc boundary layers.*

Large eddy simulations have shown that a critical region in determining when decoupling of Sc will occur is in a thin layer of unsaturated air just below cloud-base, where the vertical buoyancy flux ($w'b$) first becomes negative. The vertical extent of the K-profiles for turbulent mixing are determined to ensure that the integrated buoyancy consumption of turbulent kinetic energy (TKE) is less than or equal to a defined fraction of the buoyancy production. This requires an accurate measure of (sub-grid) cloud base height and to also include this thin unsaturated layer in the calculation of the buoyancy consumption integral. The 8A BL formulation suffered from two problems. First the model's diffuse cloud fraction across cloud base caused problems in determining cloud base height, generally diagnosing it too low. Secondly, the 8A scheme only recognises buoyancy consumption if the entire integral over the mixed layer is negative. Often positive buoyancy production above cloud base will be larger than the (negative) buoyancy consumption below leading to a positive integral.The 8B scheme attempts to deal with these issues as follows

- More accurate determination of cloud base - this is calculated using the adiabatic ql (or qf) gradient to find where ql becomes zero. In 8A this extrapolation is done from the level which satisfied C_F (cloud fraction) <SC_CFTOL (threshold value). This extrapolation has been revised to be done from the lowest level where C_F=1 (or the level with the maximum C_F)
- C_F is taken to be uniform within the cloud layer (and zero below the defined cloud base). C_F enters into the calculation of buoyancy flux.
- The integration of vertical buoyancy flux ($w'b$) is now performed over the cloud and sub-cloud layers separately.

a.2 *Surface layer integration of vertical buoyancy flux, $w'b$.*

The K profiles have a different functional form in the surface layer from that in the mixed layer, and hence the surface layer is treated separately. In the 8A BL version the surface-layer vertical buoyancy flux integration is only performed up to the lowest model θ level, assuming $w'b$ is constant over that interval and equal to the surface flux. The 8B scheme assumes $w'b'$ is linear between the surface flux value and zero at $z_{w'b=0}$ (found by linear interpolation across levels where the dry buoyancy jump in the flux integral calculation becomes negative). This is applied for z less than z_i/10 (z_i is height of mixed layer)

a.3 *Revised mixed layer height (z_h) definition for momentum diffusivity profiles (K_m)*

In 8A the mixed layer height used in momentum K-profiles (K_m) was defined as $z_h = z_{ntml+1/2}$, where z_{ntml} is the height of the turbulent mixed layer defined at one of the discrete model levels. For heat K-profiles (K_h) the z_h used is that from the sub-grid diagnosis. This discrepancy has been removed and both momentum and heat K-profiles use the sub-grid definition of z_h.

a.4 *Revised calculation of net radiative flux divergence in entrainment parametrization.*

The net radiative flux divergence is used in the entrainment parametrization and in the calculation of K_h^{Sc} via a radiative velocity scale V_{rad}. In the 8A scheme the net radiative divergence is calculated from the SW and LW heating rates. The limited vertical resolution of the model means that these heating increments are very coarse at cloud top and tend to cancel each other excessively during the day, switching off entrainment and top driven turbulent mixing. A more accurate estimate of the net radiative divergence is obtained in the 8B scheme by assuming that SW and LW radiative fluxes at a given height, z, have an exponential shape dependent on the liquid water path (LWP) above z (see Lock (2003b) for details).

a.5 *Correction to the specification of the surface friction velocity.*

An error was found in the expression for the surface friction velocity. The equation defining the surface friction velocity involves a term which is the square of the lowest layer wind shear. This had been coded incorrectly as the depending on the wind shear, and not its square. The surface friction velocity is used to scale the non-local mixing in unstable conditions (both the diffusion coefficient profiles and the entrainment rate). Therefore entrainment and boundary layer mixing could be significantly underestimated in unstable boundary layers. However, firstly, it is only in the near-neutral limit that u* makes a significant contribution (otherwise the convective velocity scale dominates). Secondly, the final diffusion coefficient is taken to be the greater of the non-local and local scheme's coefficients and the local scheme is not affected by this error. In the neutral limit both would be expected to give similar values so it is possible the local scheme has been compensating for this error. Impacts of this correction are discussed in section 4i.2.

b Revisions to large-scale precipitation microphysics (version 3C).

The microphysics and large-scale precipitation parametrization as implemented in cycle G27 is described in Wilson and Ballard (1999). It represents the following microphysical processes (i) fall of ice and rain under gravity, (ii) primary nucleation of ice particles by heterogeneous and homogeneous nucleation, (iii) deposition and sublimation of ice, (iv) aggregation of ice, (v) growth of secondary ice splinters by the Hallett-Mossop process, (vi) riming of ice by liquid water or rain drops, (vii) melting, (viii) evaporation of rain, (ix) collection of cloud droplets by raindrops, and (x) production of drizzle by the collision/coalescence mechanism. The revised 3C scheme includes a large number of changes as outlined below and is described in more detail in Wilson and Forbes. (2004):

b.1 *Improved autoconversion of cloud liquid water to rain*

Part of this change is to allow aerosols to influence the autoconversion characteristics of clouds. The current 3B scheme has a minimum liquid water content threshold (q_{cl0}) for autoconversion to occur based on specified values of the number concentration (n_L) over land/sea and a specified radius of water droplets. In the new 3C scheme q_{cl0} is redefined as the liquid water content such that the number concentration of particles of radii 20μm or larger is 1000 m-3. This leads to a new expression of q_{cl0} as a function of n_L. In the global NWP model n_L is prescribed over land and sea as for 3B, but the values in the 3C scheme have been reduced by half over land and one third over the ocean. This means that the autoconversion process now operates more readily in the 3C scheme compared to the 3B. The parameter n_L can depend on sulphate or murk aerosol if these are enabled in the UM.

b.2 *A 'consistent' sub-grid model for vapour, liquid, ice and rain contents.*

To represent heterogeneity in cloud and precipitation fields the 3C scheme divides the grid-box into eight regions representing the possible states of presence or absence of ice, liquid water and rain. The transfer processes are then solved for the eight possible partitions, assuming uniform distribution of ice, liquid water or rain over the parts of the grid-box they cover. The 3B scheme only took account of sub-grid variations for certain processes such as calculating the fall speed of ice.

b.3 *A sub-grid model for the rain variable*

Parametrization of the fraction of the grid-box covered by rain, rather than assuming rain falls uniformly over the whole grid-box.

b.4 *Framework in place for the definition of raindrop size distributions as gamma functions*

See Wilson and Forbes. (2004) for details.

b.5 *Two particle distributions to describe the ice spectra*

The 3C scheme allows for two distributions of ice particles to represent the 'observed' large (aggregates) and small (ice crystal) particle modes. There remains only one prognostic ice variable, but this is split within the microphysics code between aggregates and ice crystals according to distance below cloud top and overall ice content. Each distribution of ice has its own density and fall speed relationships.

b.6 *Revised nucleation of ice*

A coding error in the application of the Heymsfield and Milosevich (1995) equation for ice nucleation has been corrected. This lowers the nucleation threshold by 10% at warmer temperatures.

b.7 *Numerical solution of ice particle fallout*

See Wilson and Forbes. (2004) for details.

b.8 *Capacitance of ice particles - differing values for evaporation and deposition*

The deposition rate has been reduced by 10% relative to the sublimation rate. This is to reflect the observation that ice particles are more ellipsoidal when subliming as opposed to growing, which means they have a greater surface area for more efficient release and capture of molecules to and from vapour than a corresponding flat surface.

b.9 *Latent heat correction to evaporation and deposition*

The latent heating/cooling during condensation/evaporation will change the value of the saturation specific humidity, reducing the amount of condensation/evaporation which can occur. A simple estimate of this effect has been implemented

b.10 *Revised ice cloud fraction.*

A change to the definition of ice cloud fraction from ice content divided by qsatwat to a function of ice content divided by qsatwat^a qsatwat1^b qsatwat2^(1-a-b) . The qsatwat1 is calculated at cloud top temperature and qsatwat2 is a fixed value. This allows ice cloud fractions to equal 1 in deep layer cloud not possible previously.

b.11 *Calculation rather than specification of ice fall speeds*

The fall speed of an ice particle is now calculated rather than specified, given knowledge of its mass diameter and shape.

b.12 *Modifications to deposition and sublimation*

This final change was not originally part of the 3C large scale precipitation. It changes the partitioning of vapour between ice cloud and clear-sky, therefore influencing the growth rate of the ice and the equilibrium amount of ice cloud that can be maintained in a grid box of a fixed moisture content.

c Changes to Saharan albedo

Comparisons between the clear-sky albedo and OLR as observed by ERBE and more recently by the GERB[2] instrument on Meteosat-8, with those simulated in the Met Office global model (UM) have highlighted discrepancies over parts of the Saharan and Saudi deserts. During July 2003, clear-sky albedo was underestimated in the UM by approximately 0.05 in these regions (see Allan *et al* (2004)). As a countermeasure a change to the specification of surface albedo has been implemented in the HadGEM1 climate version of the Unified Model and is tested here in the global NWP model. See section 4i.1 for further details.

d Restructured convection code, corrections, and change to CAPE adjustment timescale.

The 4A version of the convection code has been restructured so that shallow, deep and mid-level convection are now called in separate subroutines. This makes code maintenance and changes easier to implement. In addition a number of coding errors have been corrected as outlined below (R.Stratton pers. comm.)

1. Ensure that increments to winds on the p-grid are correctly coded for multiple sweeps of convection. (ars5f601.mf77)
2. Correct error in calculation of shallow cumulus convective momentum transports (CMT) - the U component of momentum flux (UW) was being used incorrectly in the V wind momentum flux equation at top of shallow convection (ars6f601.mf77)
3. Correct for missing exner function calculating parcel temperature after entrainment (ars7f601.mf77).
4. Correct the density weighting to cloud base stress in CMT (ars9f601.mf77).

[2]Geostationary Earth Radiation Budget

Tests of the restructured code and corrections in an aqua-planet run showed small impacts (M. Willet pers. comm.). The final change was a reduction of the default CAPE timescale from 1 hour to 30 minutes (Note: the RH based CAPE closure used operationally means that CAPE timescale can be shorter than 30 minutes if the column comes close to saturation). This change is not currently in the HadGEM1 climate model which retains a 1 hour CAPE adjustment timescale. The impacts of the convection changes are further discussed in section 4i.3.

e New geopotential height diagnostic below orography.

The current methodology for deriving geopotential heights (z_{sub}) below orography uses a temperature (T_m) at the first model level (z_m) > 2km above the surface (z_0). This is then extrapolated using a standard lapse rate ($\gamma_s = 6.5K/km$) to give a value, T_0, at the surface as follows.

$$T_0 = T_m + \gamma_s(z_m - z_0), \tag{1}$$

T_0 is then used in the thickness equation (eq. 2) along with the surface pressure (p_0) and standard lapse rate, to derive the height of the required pressure level (e.g. 1000hPa) below the orography.

$$z_{sub} = z_0 - \frac{T_0}{\gamma_s}\left[\left(\frac{P_{sub}}{P_0}\right)^{\frac{R\gamma_s}{g}} - 1\right], \tag{2}$$

This technique was devised to avoid large diurnal variations in thickness caused by extrapolating the surface temperature. However, it tends to overestimate the thickness in stable situations where there is an inversion and the surface temperature can be much colder than that suggested by the extrapolated value. An alternative algorithm has been suggested by Tim Hewson and is tested here. As in the previous method the new algorithm assumes the layer below 2km has a standard lapse rate of 6.5 K/km but an additional constraint is that this layer has the same thickness (and hence mean temperature) as modelled. In place of equation 1 we use equation 2 with thickness $z_m - z_0$ to derive a value of T_0. We then derive z_{sub} as in the previous algorithm.

3 Testing Strategy.

The following trials of the proposed changes have been carried out

1. 5 winter (Dec. 2003 - Feb. 2004) and 5 summer (Jul-Sep 2003) case studies run from reconfigured operational analyses - these are used to test each of the changes independently.
2. Summer trial (21 July - 21 August 2003) with 3D-Var ***without*** convection changes.
3. Summer trial (21 July - 21 August 2003) with 3D-Var ***including*** convection changes
4. Winter trial (21 December 2003 - 21 January 2004) with 3D-Var
5. Winter parallel trial with 4D-Var (14 December 2004 - 18 January 2005)

The control run uses the scientific formulation as operational in model cycle G31 from March 2003 onwards and is Unified Model version 6.0 (implemented as cycle G31_6.0 in April 2004).

4 Results from case study tests.

In sections 4a-h we discuss the impacts the full package, the 3C large scale precipitation, and the 8B BL scheme including the correction to surface friction velocity. The impacts of the increased Saharan albedo, the correction to surface friction velocity, and changes to convection are dealt with separately in

sections 4i.1, 4i.2, and 4i.3 respectively. The dates of the five winter and five summer case studies are given in table 1. Most of the diagnostics shown are 5 case averages for winter and summer.

Winter	Summer
17.12.2003	19.06.2003
31.12.2003	02.07.2003
14.01.2004	15.07.2003
28.01.2004	29.07.2003
11.02.2204	01.09.2003

Table 1: *Initial dates for case studies. They are chosen to be ~2 weeks apart to try and ensure each case study is independent from the next in terms of sampling synoptic regimes.*

a Precipitation and Evaporation.

Figure 1 shows the impacts of the individual components on the accumulated 5-day total precipitation for the Dec-Feb and Jun-Sep case studies. In both seasons the full package shows a decrease in precipitation over the tropical oceans and an increase over tropical land, including tropical islands such as around the Maritime Continent, which is well known as a region of precipitation deficit in the Unified Model (Neale and Slingo (2003)). Both of these changes act to correct known systematic errors in Unified Model tropical precipitation. Over the tropical oceans the biggest contribution is from the 8B BL scheme (Fig. 1). The possible physical mechanism for these changes are discussed in section 4g. Over tropical land both the 8B BL and the 3C LS precipitation contribute to the increased precipitation, although neither change fully accounts for the impact seen in the full package. The changes to the CAPE adjustment timescale is playing a role here and this is discussed further in section 4i.3.

In the extra-tropics the signals are less systematic with both increases and decreases in precipitation (Fig. 1). If we split the precipitation into convective and large scale components for Dec-Feb (Fig. 2) we see a more systematic signal in the extra-tropics . There is increased convective rainfall in the NH and SH storm tracks at the expense of the large-scale rainfall. This signal comes entirely from the 3C large-scale precipitation scheme. The tropical change in precipitation is almost entirely due to changes in the convective rainfall with largest contribution over the oceans from the 8B BL scheme. There is some large scale rainfall over land in the tropics, and this has been systematically reduced in the 3C scheme (compensated by increased convective rainfall) but systematically increased in the 8B BL scheme. The package shows a small increase in large-scale snow amounts in the Pacific, Atlantic, and SH storm tracks, and also over Europe, which are partly offset by decreases in convective snowfall (Fig. 3). The 3C large-scale precipitation scheme accounts for these changes in snow (not shown).

Finally we consider the zonally averaged hydrological cycle over land and ocean (Fig. 4). Over land both the precipitation and evaporation are increased in the tropics by up to 10%. Over the ocean the precipitation over the equator is reduced by 10% and the evaporation shows decreases in most latitudes. Averaging over all points the land and ocean signals tend to cancel (not shown).

b Clouds and Radiation

The largest changes in total cloud cover are reductions over the tropical and subtropical oceans and over the poles (Fig. 5). In the extra-tropics we see both increases and decreases, although there is some suggestion of a systematic increase in cloud over land (see particularly over the western U.S. and Asia). The decrease in cloud over the poles is dominated by the change to the 3C large-scale precipitation scheme. There is an increased tendency to form ice in the 3C scheme relative to the 3B scheme which is due to the parametrization of smaller ice particles in the 3C scheme. This ice then falls out on short

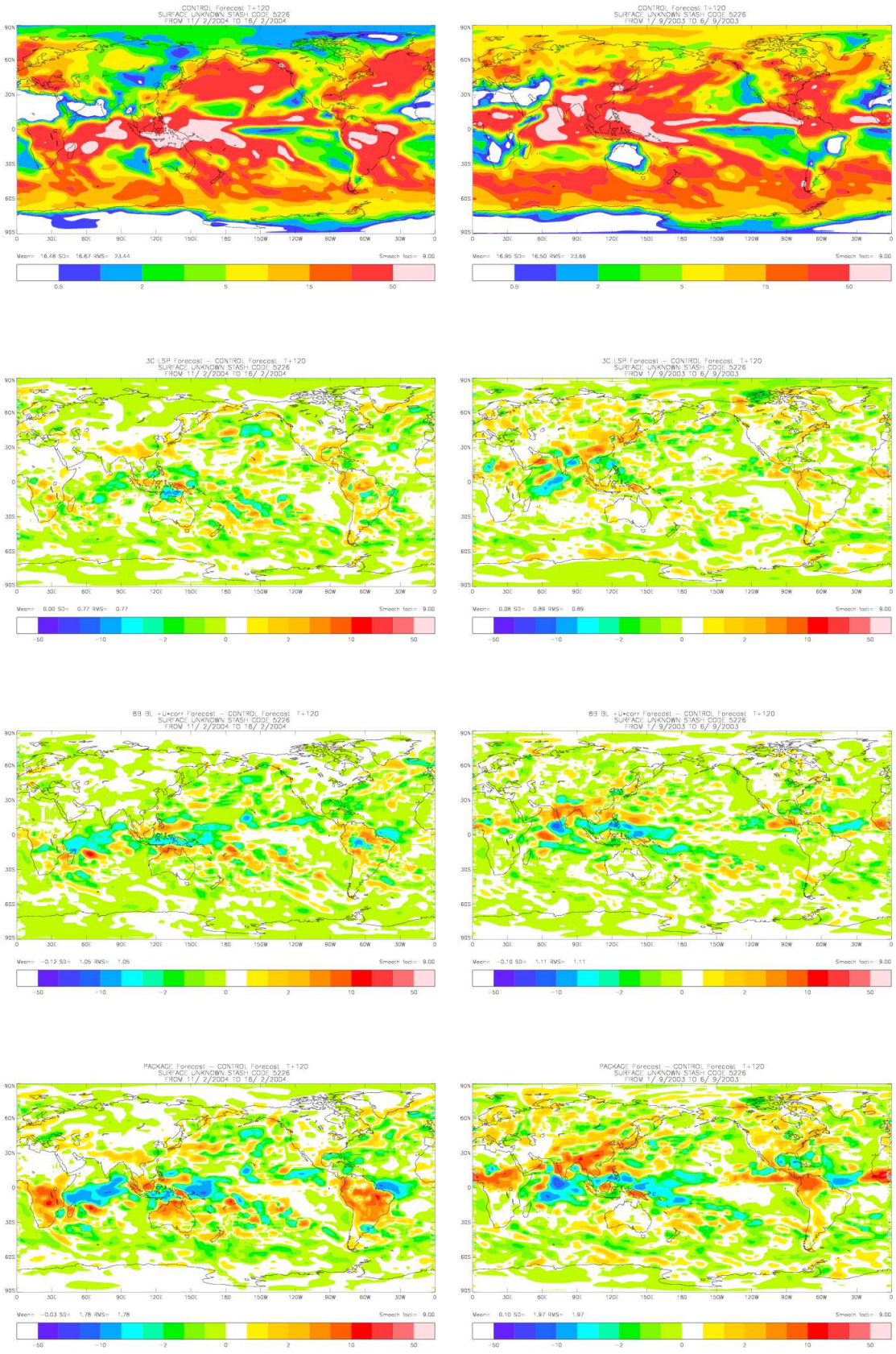

Figure 1: *Impacts on day 5 (accumulated) total precipitation. Control forecast precipitation for Dec-Feb (left) and Jul-Sep (right) in top row, Impact of 3C LS precipitation microphysics (2nd row), impact of 8B BL scheme & correction to U* (3rd row), and impact of full package (bottom row)*

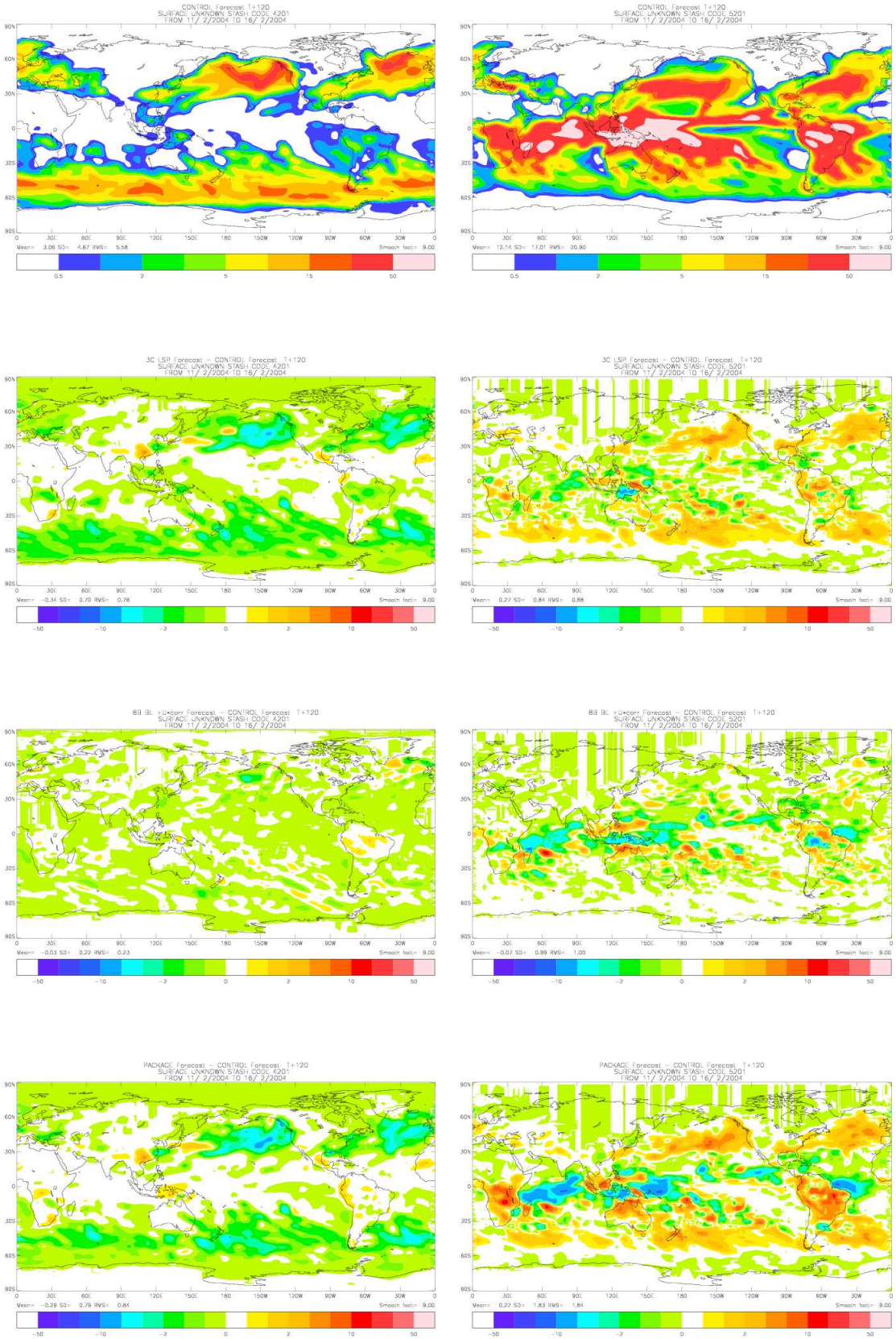

Figure 2: *Impacts on day 5 (accumulated) large-scale (left panels) and convective (right panels) rainfall during Dec-Feb. Control forecast in top row, Impact of 3C LS precipitation microphysics (2nd row), impact of 8B BL scheme & correction to U* (3rd row), impact of full package (bottom row)*

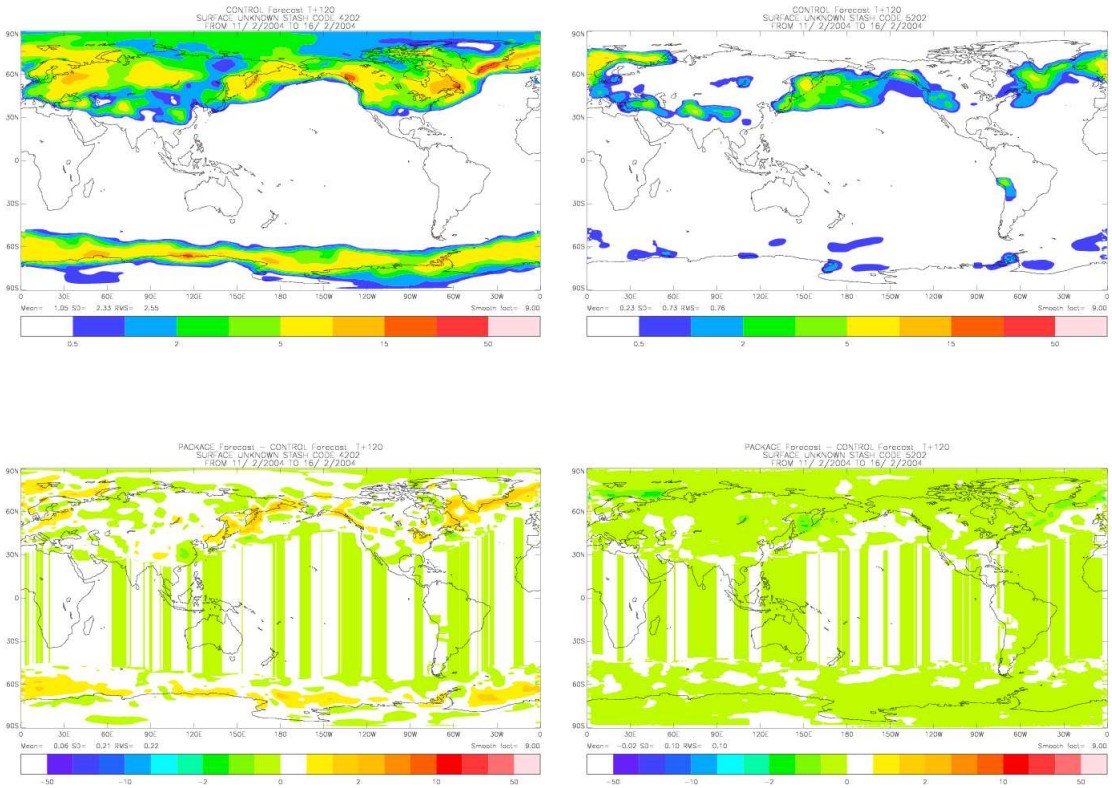

Figure 3: *Impacts on day 5 (accumulated) large-scale (left panels) and convective (right panels) snow during Dec-Feb. Control forecast in top row, and impact of full package (bottom row)*

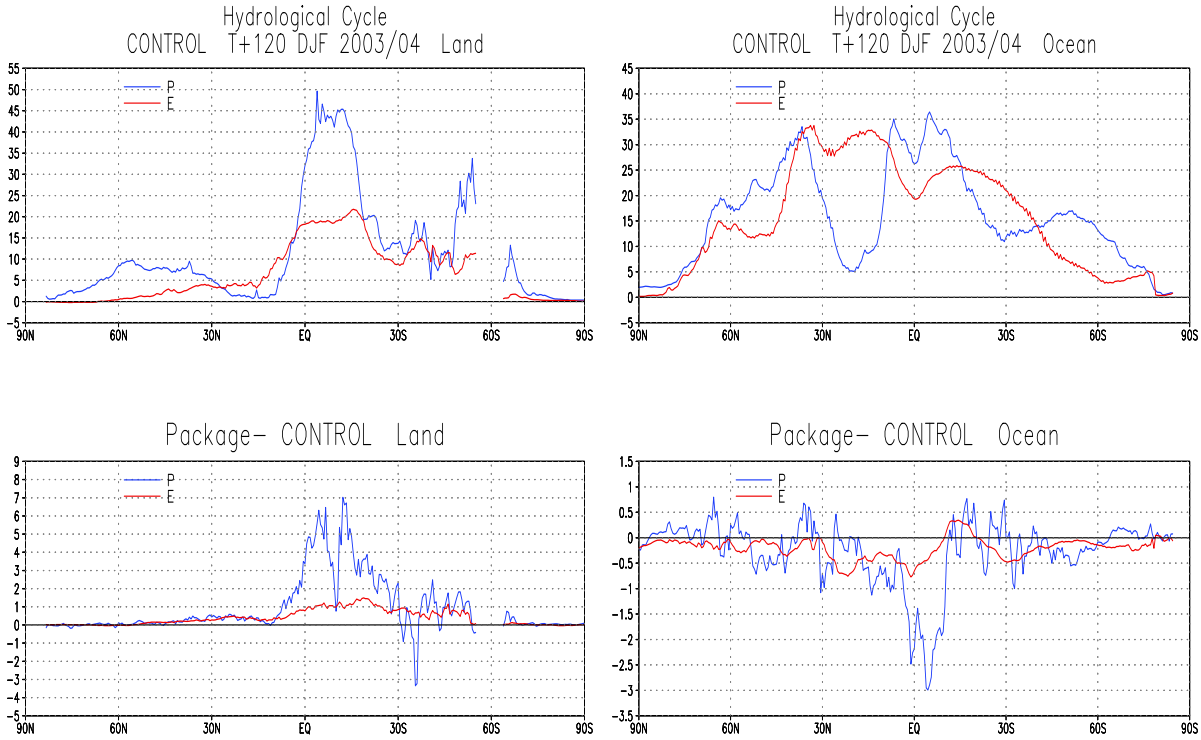

Figure 4: *Zonally averaged 5-day accumulated precipitation (P) and evaporation (E) for the Control experiments over land and ocean (top panels). Differences (Package- Control) in land and ocean P and E (bottom). Units mm/day. Results are for the Dec-Feb case studies.*

timescales leading to a reduction in cloud. The 3C precipitation scheme also shows a reduction in total cloud cover in the tropics, particularly in the regions of active oceanic convection such as the west tropical pacific. The 8B BL scheme shows reductions in cloud cover mainly over the subtropical and tropical oceans. Comparisons against ISCCP[3] global mean cloud cover suggest that the model already underestimates cloud cover and the HadGEM1 changes make this situation slightly worse (see Table 2). Of course there is no guarantee that correct cloud cover will mean the correct cloud radiative properties.

	Dec-Feb	Jul-Sep
ISCCP	67	66
Control	58	57
3C Large scale precip	55	55
8B BL	56	55
Full Package	54	54

Table 2: *Global mean cloud cover (%) for ISCCP DJF and JJA (1985-89) and global Unified model for Dec-Feb and Jul-Sep case studies.*

A more detailed analysis similar to that carried out by Webb *et al* (2001) would be required to unravel the role of cloud amounts vs. cloud optical thicknesses in determining the cloud-radiation errors in the NWP model.

The vertical distribution of large-scale cloud changes is shown in figure 6. The reductions in tropical and subtropical cloud in the full package are largely from changes in low cloud, with a significant

[3]International Satellite Cloud Climatology Project.

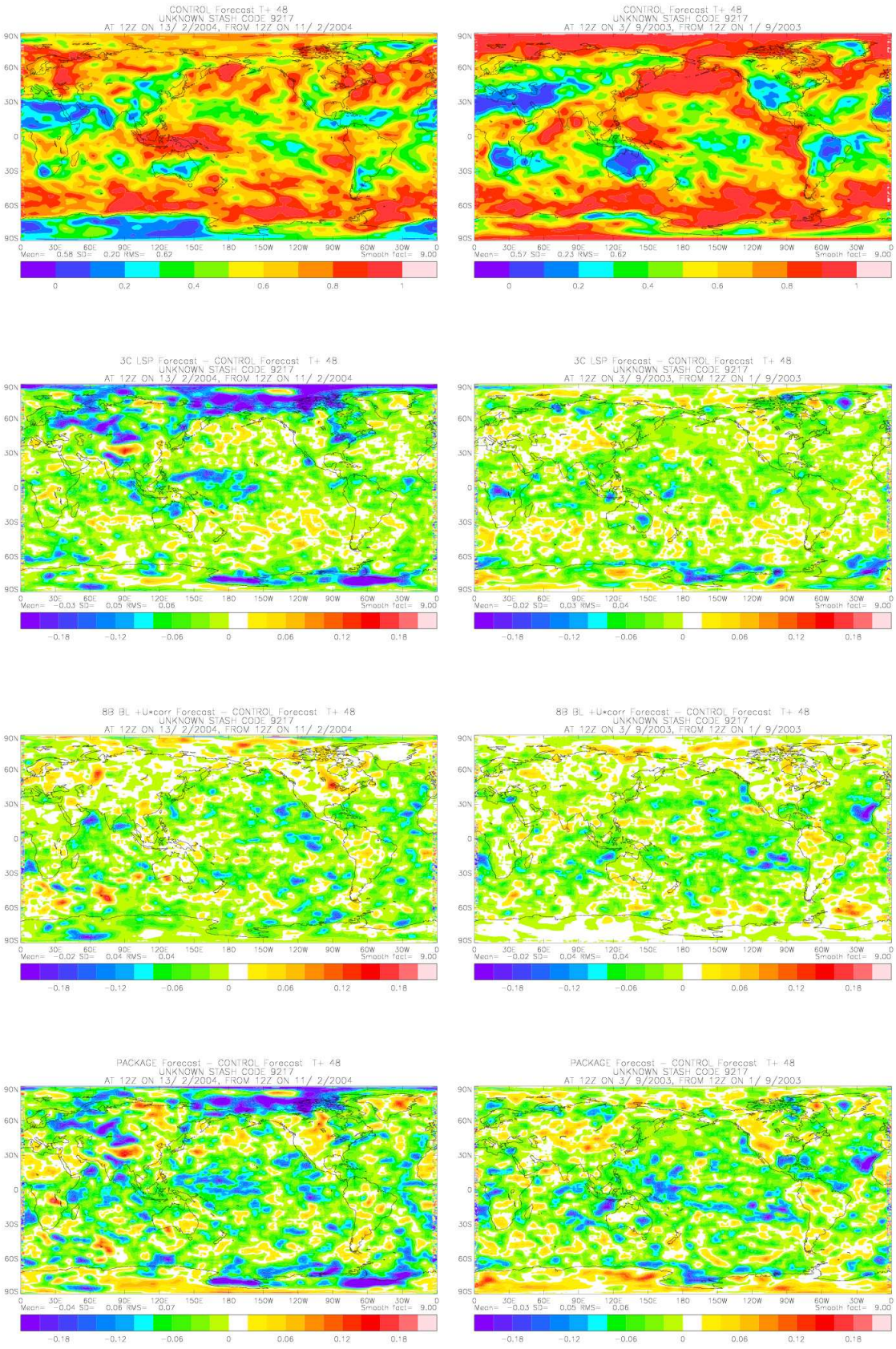

Figure 5: *Impacts on total cloud fractions at day 2 . Control forecast cloud for Dec-Feb (left) and Jul-Sep(right) in top row, Impact of 3C LS precipitation microphysics (2nd row), impact of 8B BL scheme & correction to U* (3rd row), impact of full package (bottom row)*

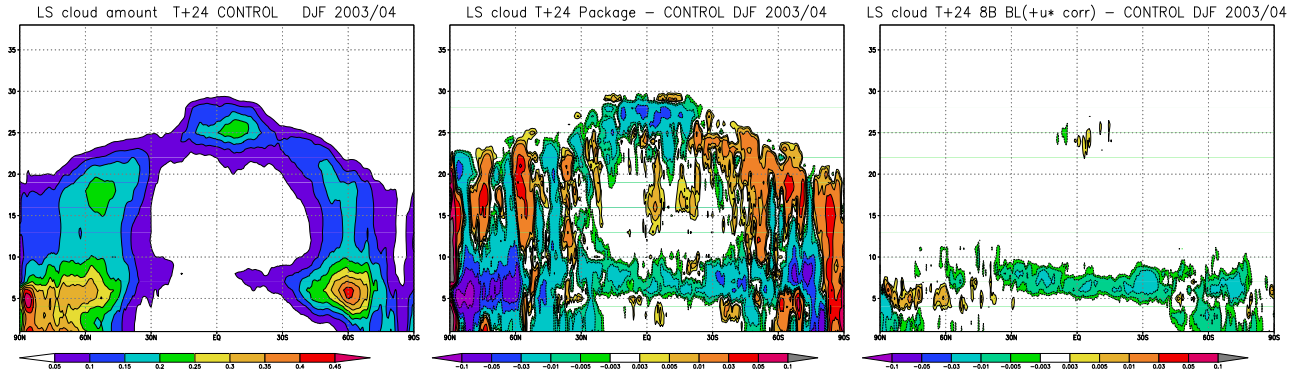

Figure 6: *Zonally averaged large scale cloud fractions as a function of model level from T+24 forecasts of control (left panel), full package - control (middle panel) and 8B BL scheme (including u* correction) - control (right panel). (*Note the irregular contour interval)*

component of the reduction coming from the 8B BL scheme (Fig. 6 right hand panel). There is also a reduction in layer cloud at the tropopause in the tropics which comes from the change to ice cloud fraction diagnosis (see section 2b.10). However, the biggest reductions are for low cloud in the polar regions dominated by the change to the 3C large-scale precipitation scheme. There are increases in cloud cover in the upper troposphere in the extra-tropics but these are typically an order of magnitude smaller than the changes in low cloud (note irregular scale in plot).

One way to partially evaluate the cloud cover is to study the top-of-the atmosphere (TOA) radiation budget. Figure 7 compares T+48 forecast radiative fluxes at the TOA with those from ERBE for 1985-89. For outgoing longwave radiation (OLR) both models show good agreement with ERBE over most latitudes, the exception being the polar regions where OLR is overestimated largely due to errors in clear sky OLR. The main differences between package and control forecasts occur in the tropics and subtropics. OLR is increased in the package due to decreases in cloud cover (clear sky fluxes do not show any change). This makes the comparisons with ERBE worse as OLR is now too large and LW cloud forcing[4] is underestimated. The net downward SW radiation is systematically larger in the package compared to the control again due to the decrease in cloud cover. The SW cloud forcing is reduced which represents improvements in the subtropics (15N-30N & 15S-40S) but degradations elsewhere. Both package and control forecasts show large errors in SW cloud forcing in the SH storm track, with the maximum in cloud forcing too broad and too far equatorward compared to ERBE. On the whole the changes to cloud are ambiguous with regard to the TOA radiation balance. We see some improvements in SW cloud forcing in the subtropics but an increase in the underestimate in LW cloud forcing in the tropics.

The other capability we have is to compare the global model TOA radiative fluxes with data from the GERB instrument on Meteosat 8. Routine comparisons with GERB are carried out under the SINERGEE project between Met Office and ESSC (see Allan *et al* (2004)). Figure 8 shows the model and GERB planetary albedo at 12 UTC for two periods; 1-17th January 2005 prior to the introduction of the new physics package and 19-31 January following the change. We must be careful in comparing these two periods not to interpret changes in radiative fluxes which are due to natural variability in weather regimes as being due to the model changes. Despite this caveat we believe there are clear signals of the model changes. The most obvious improvement is the increase in Saharan albedo in the model after 18th January, bringing it in much closer agreement with GERB (Fig. 8). Over the Atlantic ocean the model suffered from an excessive albedo in the first half of January, but following the change is in much closer agreement with GERB. The improved albedo is due to the reduced low cloud over the subtropical

[4]LW cloud forcing = OLR(clear) - OLR

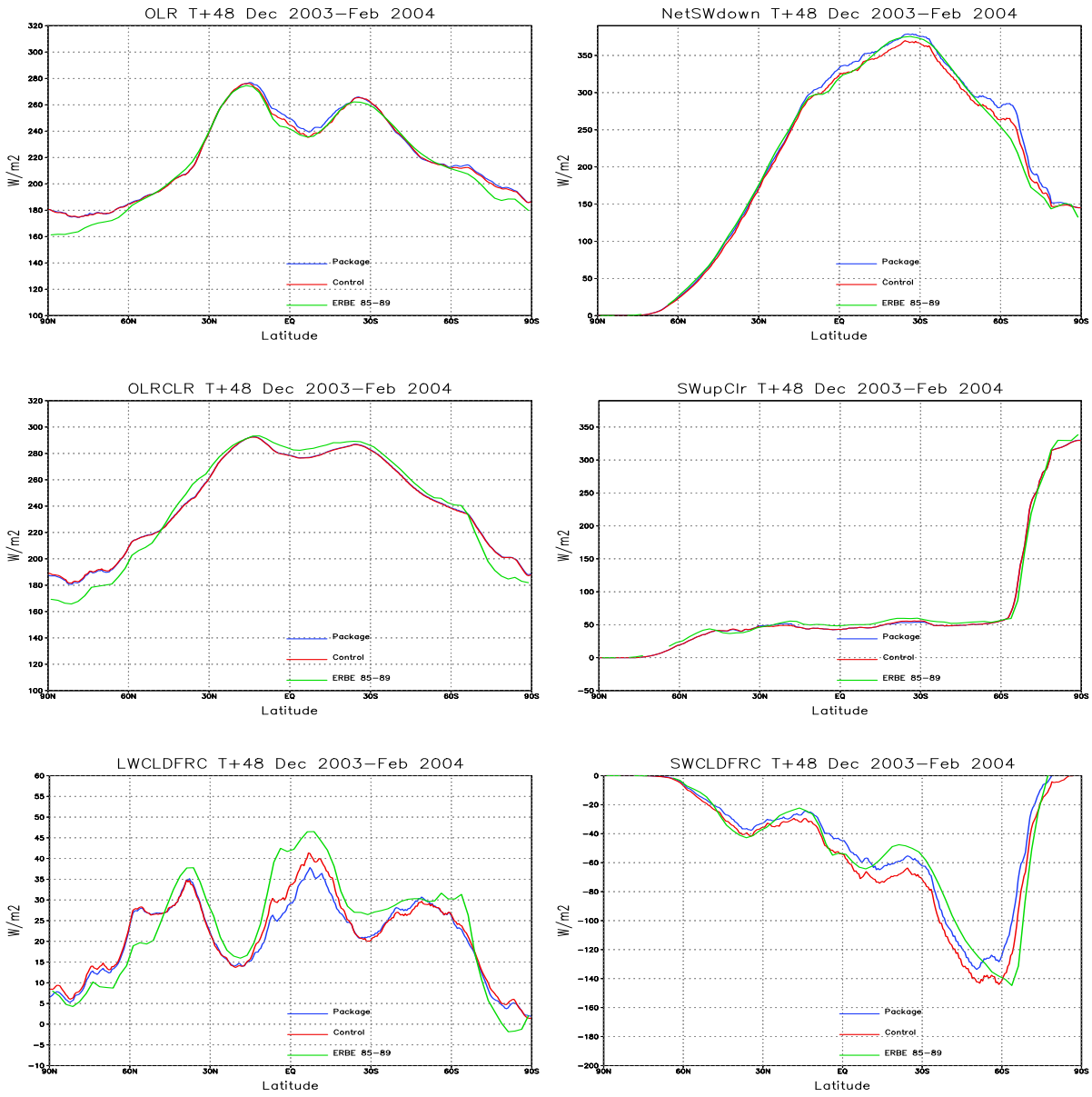

Figure 7: *Zonally averaged radiative fluxes at top-of-atmosphere from T+48 forecasts of Package and Control vs ERBE data from 1985-89. OLR (top left), Net SW down (top right), clear sky OLR (2nd row left), clear sky outgoing SW (2nd row right), LW cloud forcing (3rd row left), and SW cloud forcing (3rd row right). Units are Wm-2.*

oceans with the new physics package (see Fig. 5). Figure 9 shows the OLR at 00, 06 and 12 UTC for the

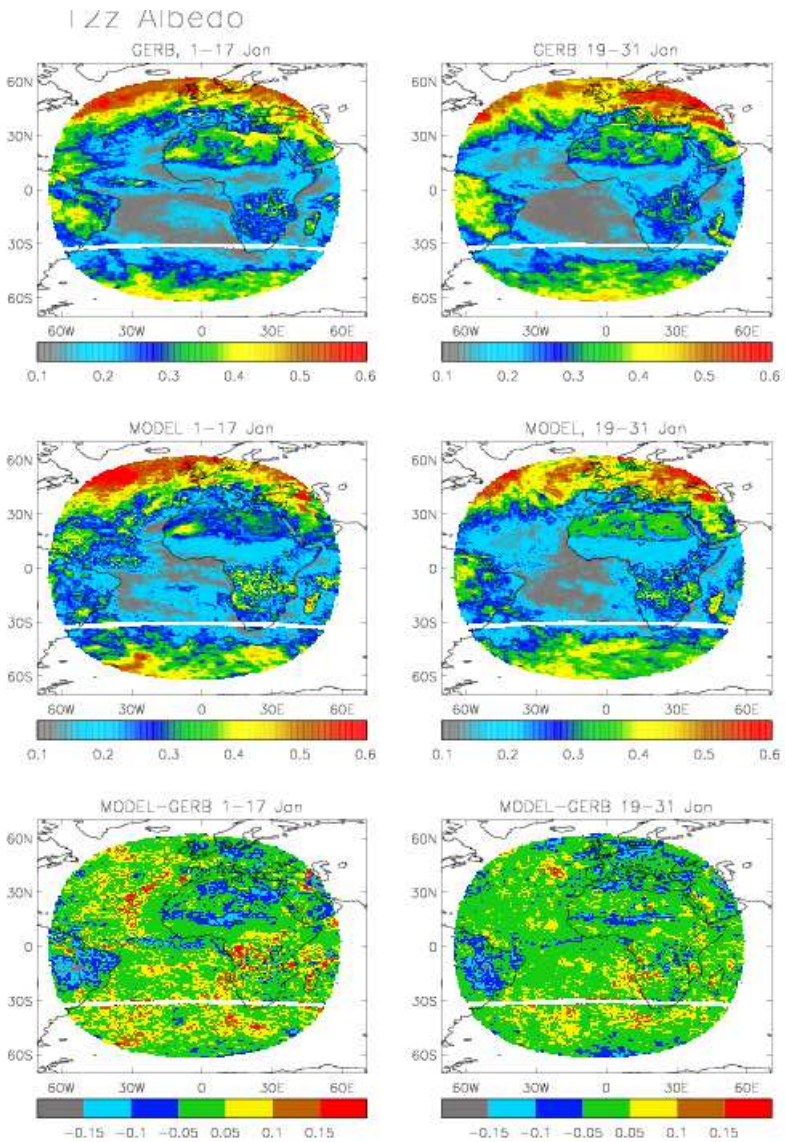

Figure 8: *Top of the atmosphere albedo at 12UTC from GERB (top), Unified Model analyses (middle), and Model- GERB (bottom). Left hand panels are for 1-17 January 2005 and right hand panels for 19-31 January 2005.*

model minus GERB. Over the Sahara we can see that prior to 18th January the OLR is too large in the model, particularly at 12 UTC. This is due to the surface absorbing to much solar radiation during the day leading to a warm bias in skin temperatures which is reflected in the OLR. The increased albedo in this region reflects more solar radiation to space, reducing the warm bias in skin temperature and OLR. The other area of improvement is in the ITCZ near the equator. For example, at 06 UTC the model was underestimating the OLR by up to 30 Wm^{-2} just off the S.American coast during the period 1-17th January. This is probably due to overactive oceanic convection producing too much cloud. The 19-31 January period shows reduced errors in this region, consistent with the reductions in tropical precipitation (and cloud) discussed earlier (see section 3a)

Finally, we consider a specific issue with cloud forecasts over Iraq which was raised by the forecasters in the OPS centre (NMC problem 182). This related to excessive low cloud and fog being forecast over Iraq during Winter and Spring (Fig.10). As a consequence daytime temperatures are suppressed by

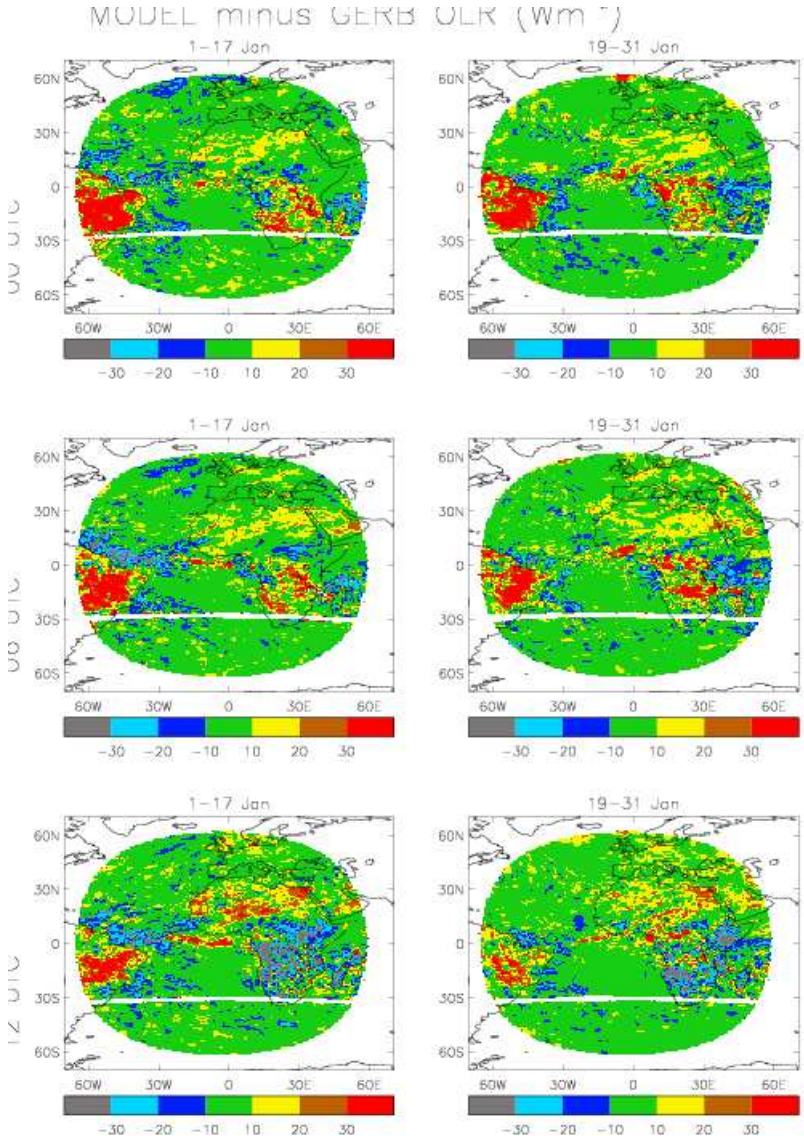

Figure 9: *Model-GERB for OLR (Wm-2) at 00UTC (top row), 06UTC (middle), and 12UTC (bottom). Left hand panels are for 1-17 January 2005 and right hand panels for 19-31 January 2005.*

several degrees. The change to the 3C large-scale precipitation scheme acts to dissipate this cloud/fog mainly via a more efficient autoconversion process. This gives much more accurate forecasts of cloud (Fig. 10) and 1.5m temperatures (not shown).

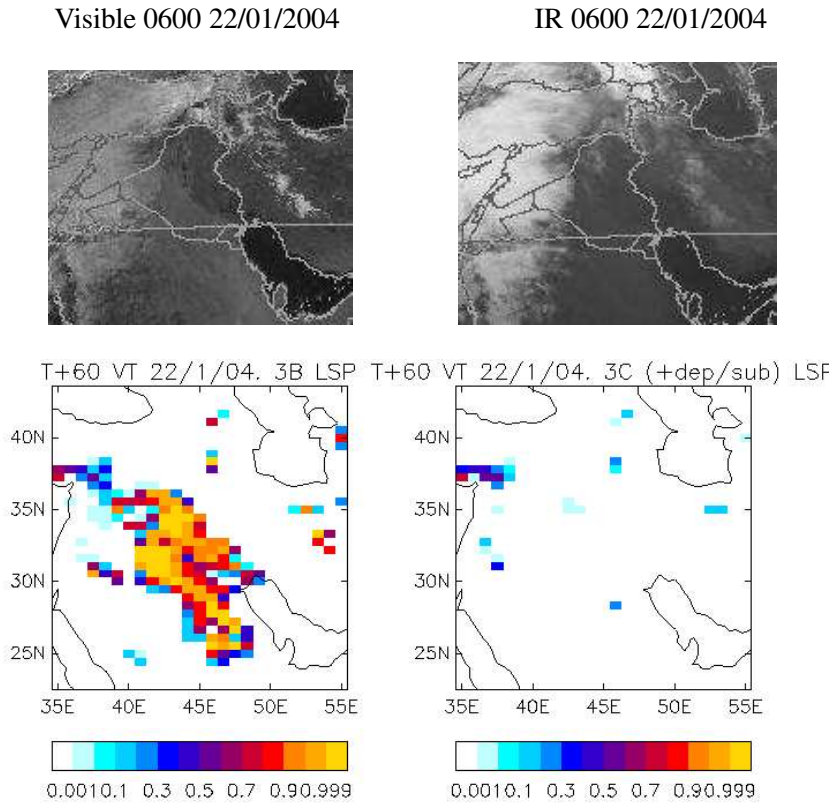

Figure 10: *Impact of 3C large-scale precipitation on fog over Iraq on 22 January 2004. The top panels show the visible and IR images from Indosat at 06 UTC and the lower panels show the T+60 forecasts of fog fraction valid at 12 UTC 22/1/2004 for 3B (left) and 3C (right) large-scale precipitation. The satellite imagery shows no indication of the fog seen in the 3B forecast. The 3C forecast removes the spurious fog.*

c Temperature.

The current day 5 temperature biases in the global NWP model are shown in figure 11 for the Jul-Sep 2003 case studies. The tropics and NH show a warming of order 1K in the mid-troposphere. There is also a warm bias in the stratosphere, near the surface in the tropics and at high latitudes in winter (SH in Jul-Sep). Elsewhere, there are cold biases in temperature, most notably in northern high latitudes, in the

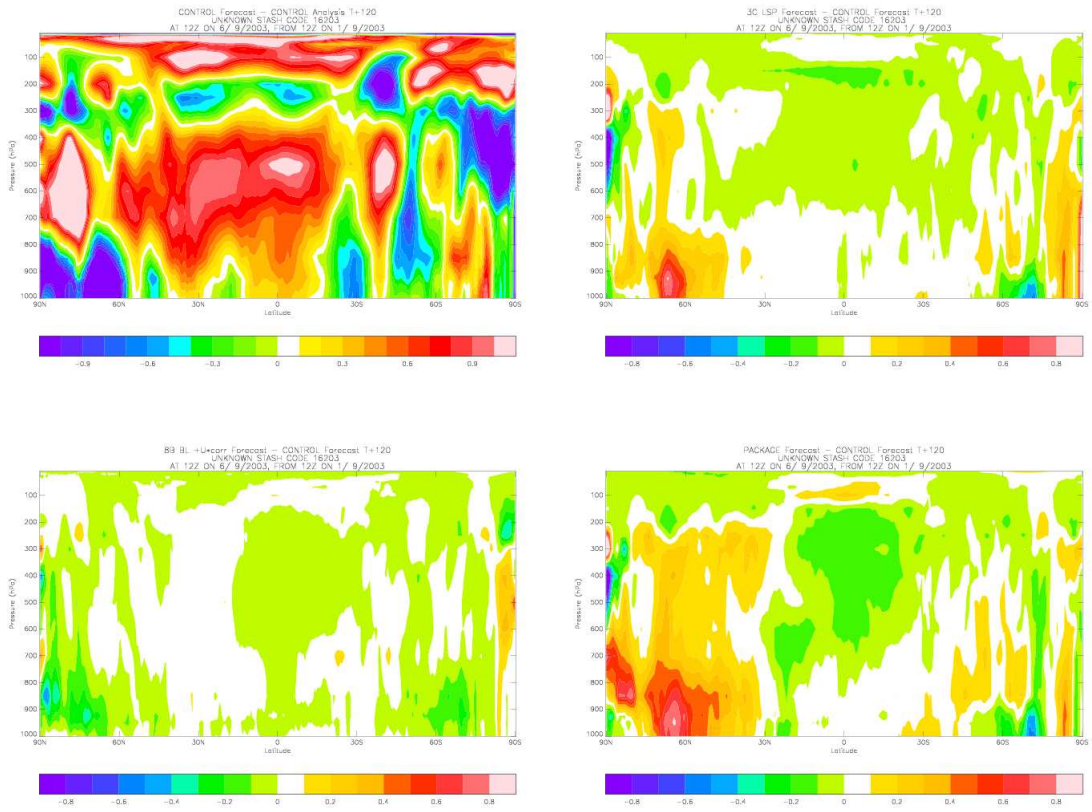

Figure 11: *Impacts on zonally averaged day 5 forecast temperatures from Jul-Sep case studies. Control forecast errors (top left), Impact of 3C LS precipitation microphysics (top right), impact of 8B BL scheme & correction to U* (bottom left), and impact of full package (bottom right).*

subtropical boundary layer and at the tropopause.

The impact of the 8B boundary layer scheme is to cool the tropics by 0.1 K in five days throughout the depth of the troposphere. This is due to reduced diabatic heating from the convection scheme (Fig. 15), consistent with reduced precipitation over the tropical oceans (Fig. 1). This gives a small improvement to the existing tropical warm bias in mid-troposphere, although the 250hPa cold bias is worse (see Fig. 14). Further cooling from the 8B BL scheme occurs poleward of 60N and 60S in the boundary layer (Fig. 11). The impact of the 3C scheme is also to cool in the tropics above the boundary layer. In the extra-tropics the 3C scheme leads to a warming. This warming seems to come from a number of complex changes to heating from the physics associated with large scale precipitation, (reduced) LW cooling , convective heating, and large-scale cloud (see next section).

The full package of changes is largely a combination of changes seen in the individual components with a broad scale cooling in the tropical mid to upper troposphere and a warming in the extra-tropics with largest changes near the surface in high latitudes. This high latitude warming near the surface is beneficial improving the verification results for 1.5m temperatures from the July-August 2003 3D-Var

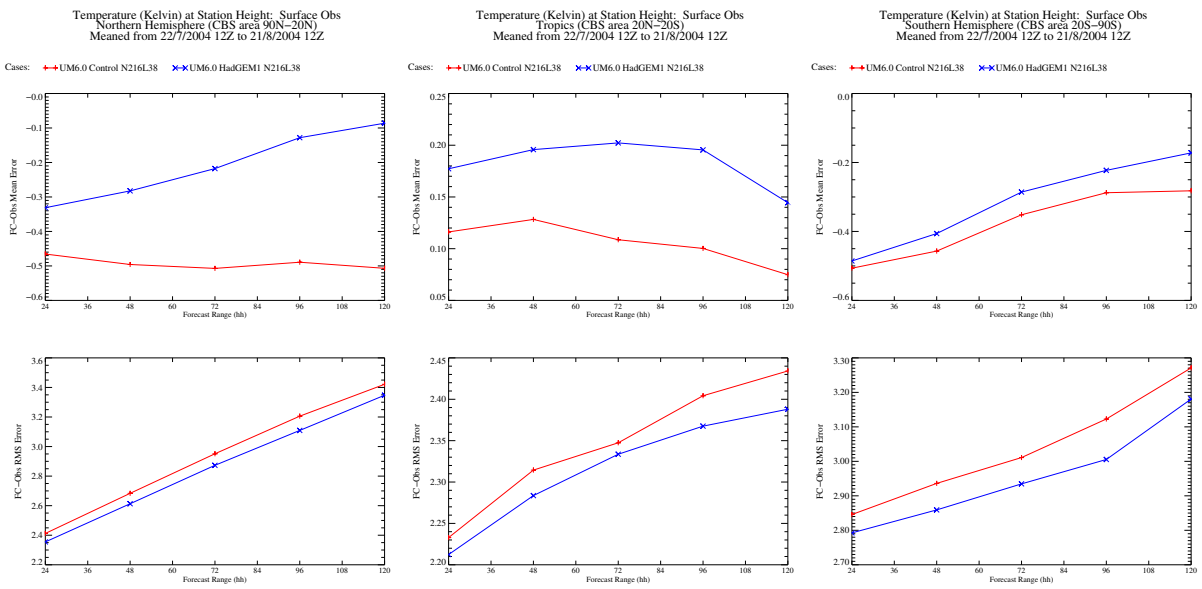

Figure 12: *Mean error (top row) and RMS error (bottom row) as a function of forecast range for 1.5m temperatures from the Jul-Aug 2003 3D-Var trial of the full package (**not** including convection changes). NH (left panels), tropics (middle panels) and SH (right panels). Verification is against SYNOPS.*

trial (Fig.12). However, in the mid-troposphere the existing warm bias is increased (Fig.13).

d Thermal Balance.

It is useful to consider the origin of the changes in temperature structure by examining the heating rates in the first 24 hours of the forecasts from each of the model's parametrization schemes (Fig. 15) . We have already inferred that the tropical cooling is linked to reduced convective heating in the 8B BL scheme and this can be seen in the convective heating increments for Package - Control. However, there is also a contribution from increased LW cooling in the tropical mid-troposphere, presumably associated with changes in cloudiness (Fig. 6).

In the mid-latitudes (30N-60N) we see a number of complex and interacting effects from changes in the model's hydrological cycle. The large-scale precipitation scheme heats in the mid-troposphere from production of precipitation and cools below this due to the evaporation of precipitation. The impact of the full package is to decrease the heating in the mid-troposphere and decrease in the cooling from evaporation of precipitation near the surface (i.e. a warming). Both are consistent with reduced large scale precipitation seen in the extra-tropical storm tracks (Fig. 2). The reduction in latent heating from large scale precipitation in the mid-troposphere is balanced by an increased heating from convection, consistent with the increased convective precipitation (section 4a). These changes are due to the 3C large scale precipitation as this signal is absent from the 8B BL scheme impacts (Fig. 16).

In the high latitudes north of 60N there is increased heating from large-scale precipitation between model layers 3 and 10 (950-700hPa) and increased cooling near the surface. This may be due to the increase in large scale snow seen in the 3C precipitation scheme (Fig. 3). The other main change is to LW heating rates. Between model level 5 and 10 we see a decrease in LW cooling locally which corresponds to regions of reduced low cloud (Fig.6).

The budget residual heating rate (parametrized + dynamics) shows the degree of imbalance between the parametrizations and dynamics in the first 24 hours of the forecast. The budget residual from the control forecasts shows reasonable agreement with the errors in the zonally averaged temperature field (Fig. 11). The *changes* in the budget residual from using the new package show a warming at all lati-

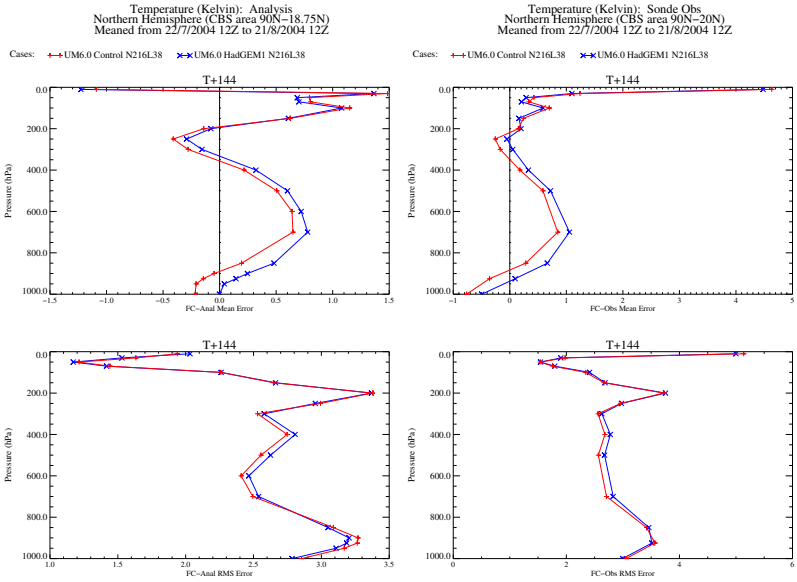

Figure 13: *Objective verification of day 6 temperatures as a function of height (pressure) from the Jul-Aug 2003 3D-Var trial of the full package (without convection changes). Top row shows the bias and the bottom row the RMS errors. The left hand panels are for verification against analyses and the right hand for verification against sondes.*

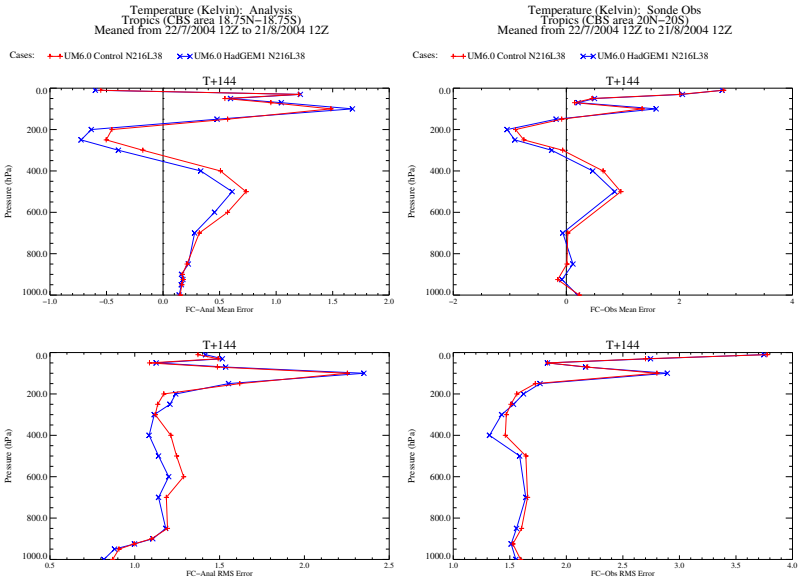

Figure 14: *As figure 13 but for the tropics.*

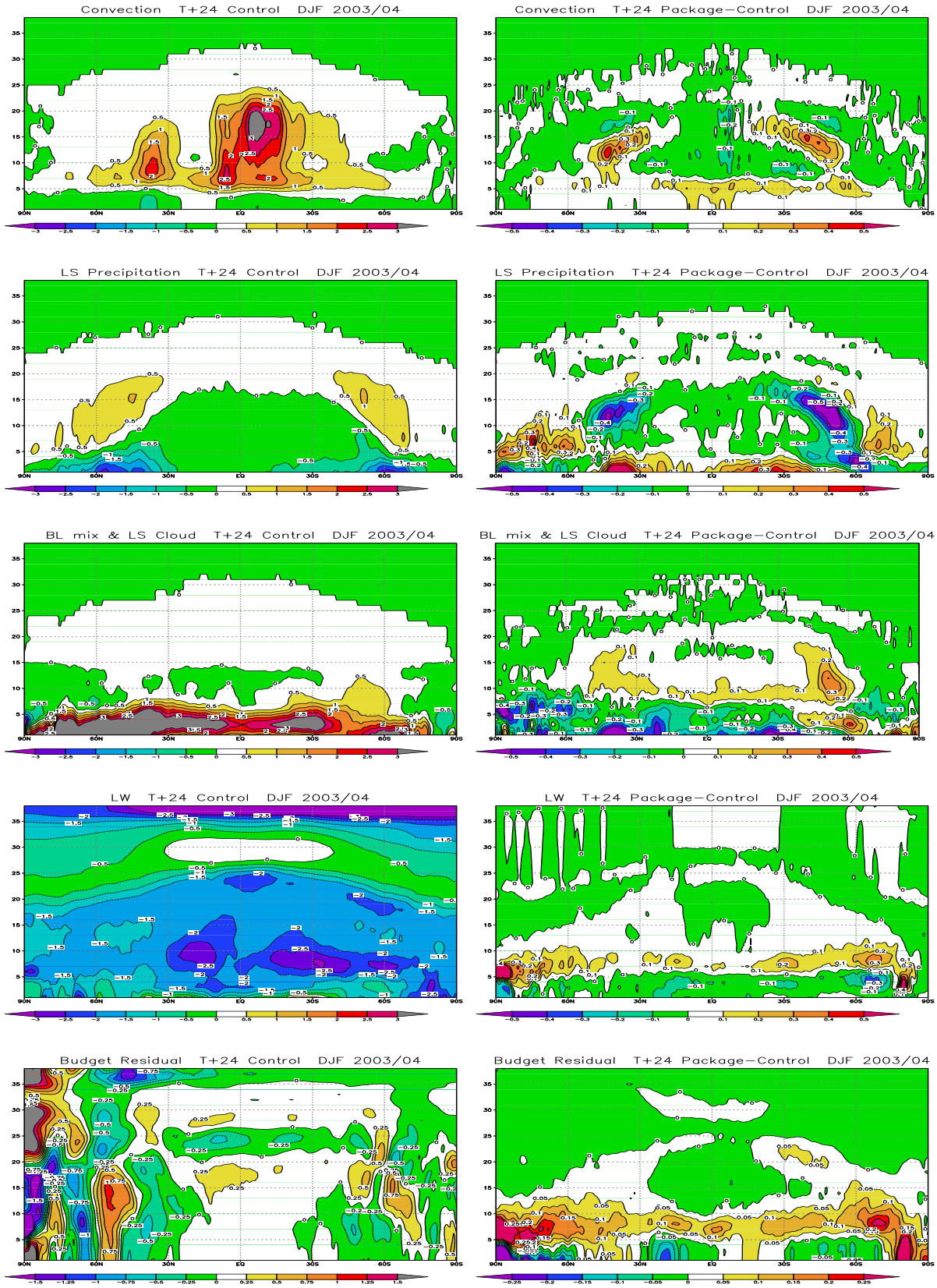

Figure 15: *Day 1 thermal balance in control forecasts and the impact of the full package. Left panels show the daily averaged and zonally averaged heating tendencies (K/day) for the some of the parametrized processes. Also shown is the budget residual which is the sum of all parametrized and dynamical contributions to the heating. The right hand panels show the forecast differences (package - control) in each of the components shown on the left.*

tudes in the upper boundary layer (levels 5-10) largest at high latitudes and with main contributions from reductions in the LW cooling and increased latent heating from the LS precipitation (increased formation of snow?). The tropical mid-troposphere cools (reduced convection heating) while the extra-tropical mid-troposphere warms slightly (complex changes between LS precipitation, convection, LS cloud and LW radiation). Overall the changes in the budget residual heating resemble those seen in the temperature field itself (Fig. 11)

Finally, we note that the changes in heating rates from the 8B BL scheme alone are generally smaller than those seen in the full package (Fig. 16). The main change is a reduction in the BL turbulent heating in the lowest model levels. This is probably due to an increase in the frequency of decoupled boundary layer types at the expense of well mixed boundary layers (section 4g). There is generally reduced mixing in the decoupled boundary layers compared to the well mixed.

e Humidity.

The current model is too moist at the tropopause in most latitudes while in the mid troposphere the model appears too dry (Fig.17). A particularly large bias is the drying at 400 hPa in the tropics with moistening above at the tropopause. This error structure may be related to particular deficiencies in the convection scheme such as errors in the detrainment of moisture and a poor representation of vertical mass flux profile in the current convection scheme. The relative humidity in the full package is drier by between 5-10% in the extra-tropics and at the tropopause at all latitudes (Fig.17). The tropics and subtropics show a small moistening. Both 8B BL and 3C large scale precipitation tend to dry the model atmosphere, but the 3C scheme has the larger impacts (not shown). Looking at the changes in specific humidity there are broadly similar signals to RH with drying over large areas of the extra-tropics and at the tropopause from the full package (Fig.18). However, in the subtropical BL the near surface humidity is higher in the new package and the tropical mid-troposphere is also moister. The higher near surface humidities may be responsible for reductions in evaporation in the subtropics (Fig. 20). The tropical and subtropical signals seem to come from the 8B BL change, whereas the drying in the extra-tropics and at the tropopause is due to the change to the 3C large-scale precipitation scheme (Fig.18).

f Surface energy balance.

In the northern hemisphere over land the 1.5m temperatures are warmer in Jun-Aug (Fig. 12) and cooler in Dec-Jan (Fig. 35) with the new physics package. These changes act to reduce existing cold and warm biases in the control in Jul-Sep and Dec-Feb respectively. To try and understand these changes we look at the surface energy budget in the package and control short-range forecasts. Figure 19 shows the zonally averaged control surface fluxes over land at T+24 and the changes (package - control) in the surface fluxes (and 1.5m temperatures). In general the changes in 1.5m temperatures follow the changes in net downward heat flux in all latitudes. In the northern hemisphere the reduction in net downward heat flux (and cooling in 1.5m temperatures) during Dec-Feb comes from a more negative net LW flux implying more outgoing and less downwelling LW radiation consistent with the reduction in cloud. This is partly offset by a small increase in sensible heating. In Jul-Sep we have the opposite signal with increasing net downward heat flux and warmer 1.5m temperatures. Increasing net downward SW radiation is responsible for these changes, again consistent with reduced cloud cover. So the improved biases in 1.5m temperatures in both seasons appear to be linked to the changes in surface radiative fluxes and the reductions in cloud, although the dominant surface radiative signals are different in each season. The largest change in the net downward surface heat flux in both seasons is a reduction between 15N and 30N in both seasons accompanied by a cooling in 1.5m temperatures. This is due to the increased albedo over the Sahara and Middle east reducing the net downward SW flux reaching the surface. The reduction in net SW flux is partly offset by reduced sensible heat fluxes and a decrease in the upwelling LW radiative flux.

The fluxes over the oceans are shown in figure 20. The net downward heat flux into the ocean is

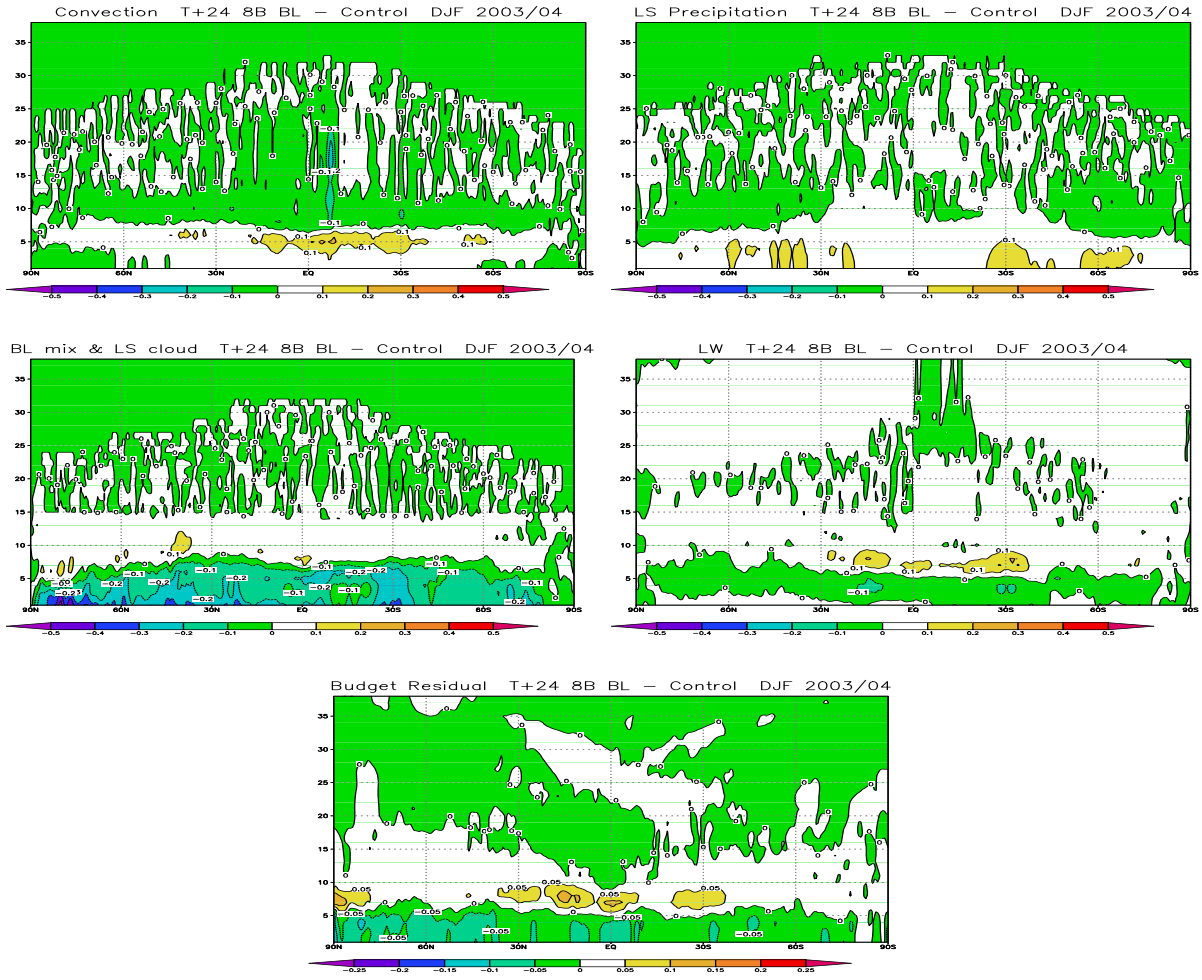

Figure 16: *Day 1 forecast differences (8B BL - control) in heating rates from convection, LS precipitation, BL turbulent mixing & LS cloud, LW radiative heating and in the budget residual (sum of all parametrized and dynamical heating rates).*

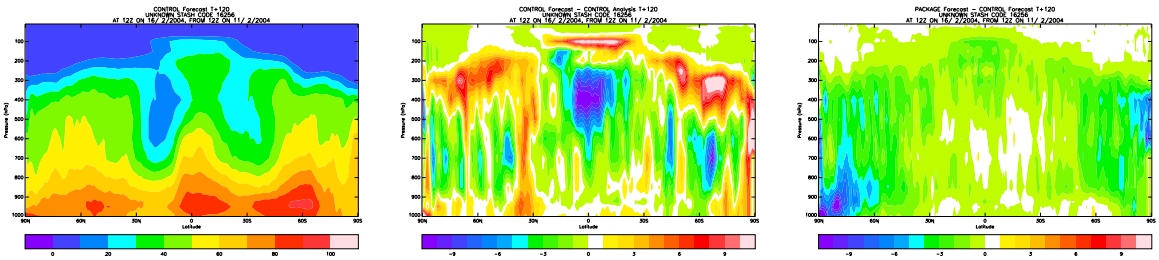

Figure 17: *Impacts on zonally averaged day 5 relative humidity for DJF 03/04 case studies. Control forecast (left), control forecast errors (middle), and impact of full package (right).*

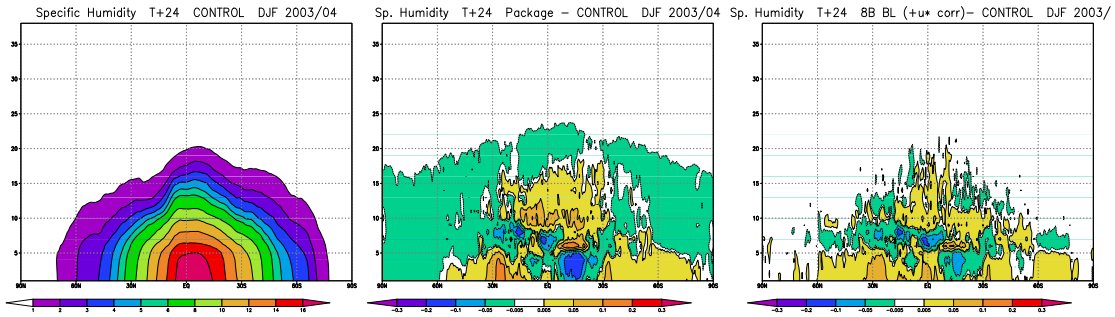

Figure 18: *As figure 6 but for specific humidity. Units are g/kg.*

increased at all latitudes with the main contribution from increased downward SW radiation (~$10 W m^{-2}$) due to decreases in cloud cover. In polar regions during winter when the net downward SW is zero the main changes are a reduction in sensible heating and an increase in the net outgoing LW radiation from reduced downwelling LW radiation due to removal of low cloud. The 1.5m temperatures over the ocean are strongly constrained by the sea surface temperatures so show very little change. This increase in downward net heat flux would have consequences for coupled models.

g Changes to Boundary Layer Types

The impacts in the 8B boundary layer scheme discussed so far arise from an altered diagnosis of the boundary layer types. The 8B BL scheme now diagnoses up to 20% more occasions of decoupled stratocumulus (BL type IV) in the subtropics, largely at the expense of the well mixed BL (type III) (Fig. 21 and 22). In the control forecasts the decoupled Sc BL type was typically was only diagnosed between 1-5% of occasions. In the Southern Ocean at 60S we also see that the stable BL's (type I) have decreased by 10% and have been replaced by decoupled Sc over a stable layer. The main impact of diagnosing more decoupled layers is in the different mixing profiles that accompanies these BL types (see Lock *et al* (2000)). It should be noted that these BL type diagnostics are for a snapshot at 12UTC so are not representative of the full diurnal cycle, particularly over land.

h Improved Tropical Winds - Rotational and Divergent flow.

Tropical systematic errors in zonal winds in the current model show too strong easterly flow in the lower troposphere and a westerly bias above this in the upper troposphere (Fig.23). This baroclinic error structure may be a consequence of excessive diabatic heating in the tropical atmosphere, consistent with tropical oceanic precipitation being too intense. The impact of the full package is to both decrease the low

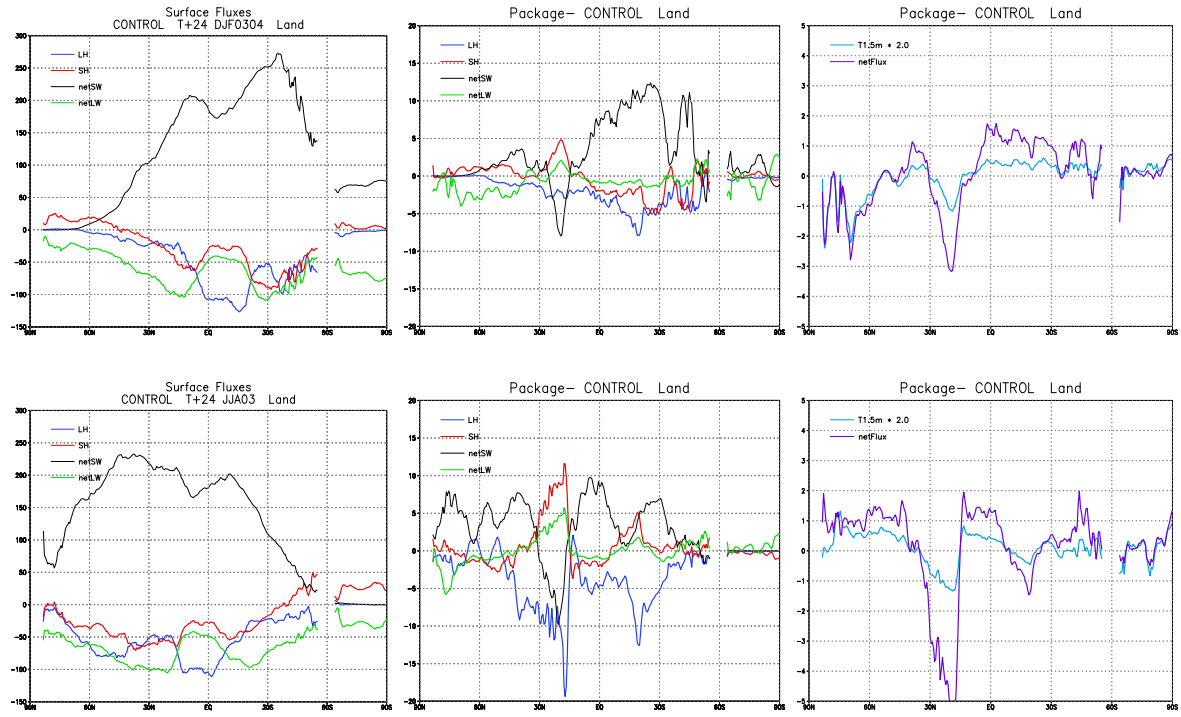

Figure 19: *.Surface energy balance over land for Dec-Feb 2003-04 (top row) and Jul-Sep 2003 case studies (bottom row). Day 1 Surface fluxes from control (left panels), day 1 forecast difference (Package-Control) in surface fluxes (middle) and net downward heat flux and 1.5m temperatures (multiplied by 2.0).*

level easterlies and reduce the westerly bias aloft. Both of these changes improve the systematic errors in tropical winds. The objective verification from the Jul-Aug 2003 3D-Var trial also shows the improved tropical low level wind speed biases and reduced RMS errors at 850 and 250 hPa for verification against both sondes and analyses (Fig.24).

The day 5 velocity potential field at 850hPa from the Dec-Jan trial trial with 3D-Var clearly shows the improvements in the tropical divergent circulation from the new physics package (Fig. 25). The error in the control forecasts is for too much low level convergence (ascent) in the west tropical Pacific and Indian Ocean with too much divergence (descent) over Africa , South America and the East Pacific. The forecast difference field (package - control) is generally in the opposite sense to the control error field showing the package is reducing these divergent circulation errors.

i Impacts of other components of the new package.

i.1 Saharan Albedo increase.

Comparisons between the clear-sky albedo and OLR as observed by ERBE and more recently by the GERB instrument on Meteosat-8, with those simulated in the Met Office global model (UM) have highlighted discrepancies over parts of the Saharan and Saudi deserts. During July 2003, the clear-sky albedo was underestimated in the UM by approximately 0.05 (see Allan *et al* (2004)). As a countermeasure a change to the specification of surface albedo has been implemented in the HadGEM1 climate version of the Unified Model and is tested here in the global NWP model. Of particular importance is the bare soil albedo. This is an ancillary file created offline from a dataset of soil properties by first categorising soils into three different types ("Light", "Medium" and "Dark"). The albedo of these soils are then dependent on the soil being "average" or "dry", which is determined by the presence of vegetation. The albedo is changed here by setting them to a fixed value of 0.4 for dry light soils, which removes the dependence

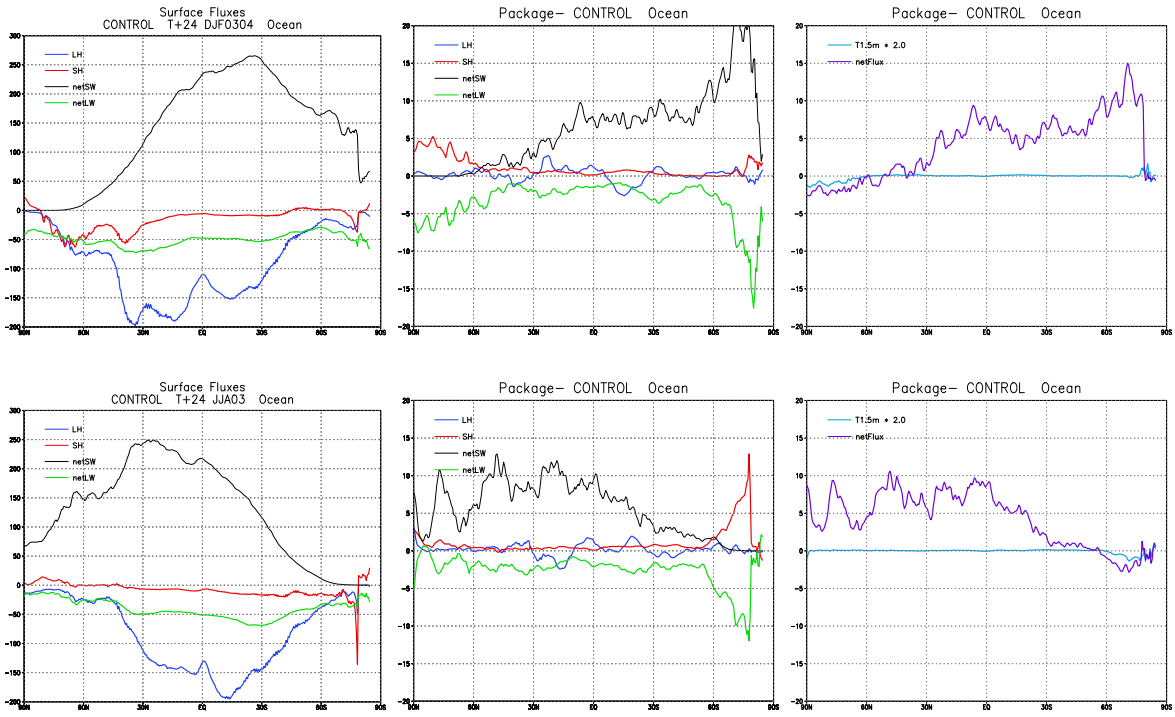

Figure 20: *.As figure 19 but for ocean points.*

of soil albedo on vegetation for this soil type. This increases the albedo over the Sahara but reduces it over the desert regions of Australia and Asia (Fig.26). It is not obvious that the decrease in albedo in these regions is correcting any particular errors. The decrease in albedo over other desert regions is removed if we use the new IGBP[5] land use dataset as it has considerably less vegetation than the WHS dataset(Fig.26). However, this new land surface dataset requires further trialling before it can go operational.

The sensible heating of the Saharan surface is reduced when the increased albedo is included in the model. Although impacts to the circulation are relatively small we do see an improved low level circulation with a spurious heat low over the region reduced due to decreases in surface heating (Fig. 27).

i.2 Correction to surface friction velocity

The impacts of correcting the surface friction velocity are consistent with increased diffusion coefficients giving stronger boundary layer mixing. Concentrating on tropical oceans, for momentum the impact in 5-day forecast tests is an increase in the near-surface wind speed and surface stress in the tropics with a reduction in wind speeds above. The boundary layer is deeper, surface moisture fluxes increase and heat fluxes decrease, and there is generally more cloud. Precipitation rates in the ITCZ increase. Although these changes oppose those seen with the 8B BL scheme alone, they are not large enough to cancel the changes from the 8B BL. The signal in a single season climate run is not so clear but surface stresses in the tropics still seem to increase.

i.3 Changes to the convection scheme.

The changes to the convection scheme (section 2d) give changes in tropical convective rainfall, with reductions over the ocean and increases over land (Fig.28). The convection changes account for most of

[5]International Global Biosphere Project

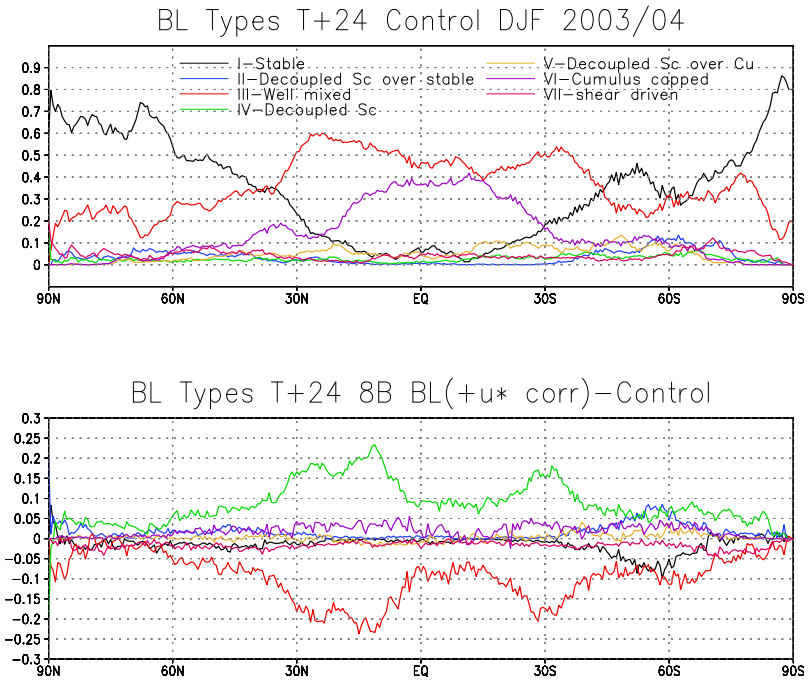

Figure 21: *Zonally averaged frequencies of BL types for T+24 control forecasts (top) and for the forecast difference (8B BL - Control) (bottom)*

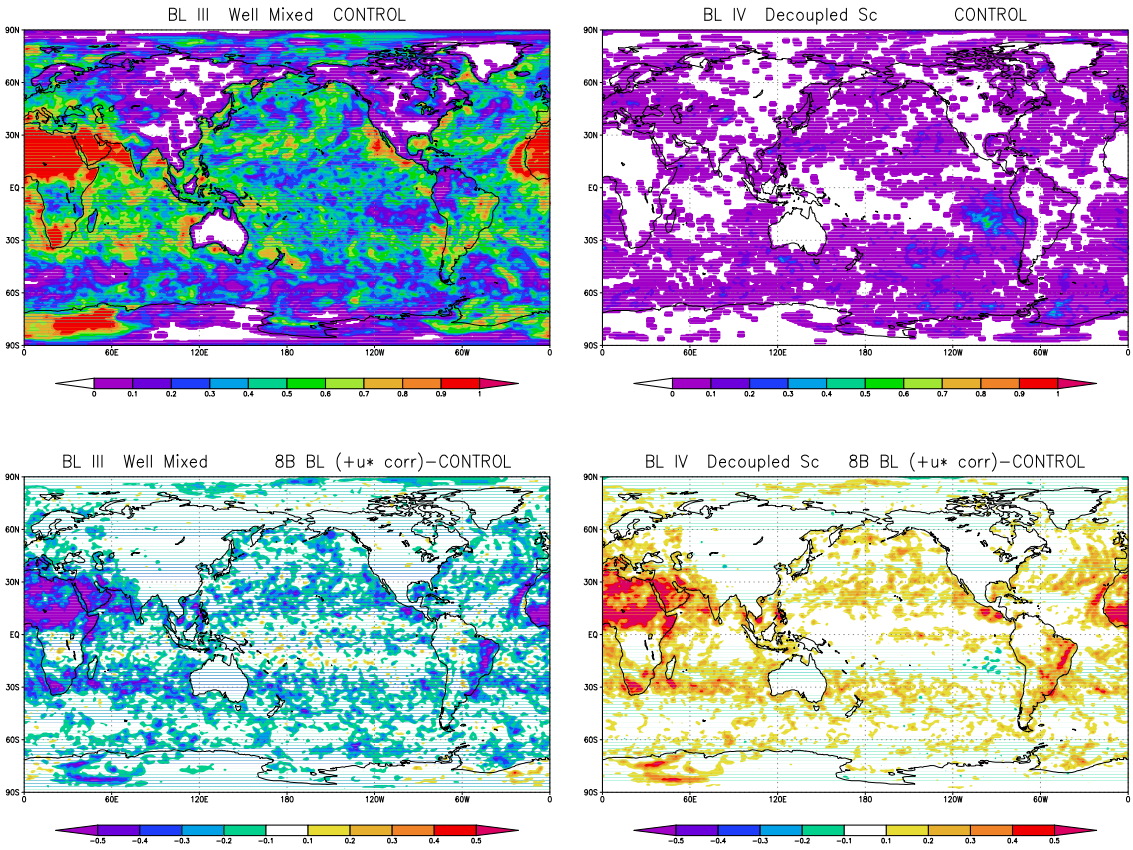

Figure 22: *Frequency of well mixed BL (type III - left) and decoupled stratocumulus (type IV - right). Top panels show the T+24 control forecasts and the bottom panels the forecast differences (8B BL - Control).*

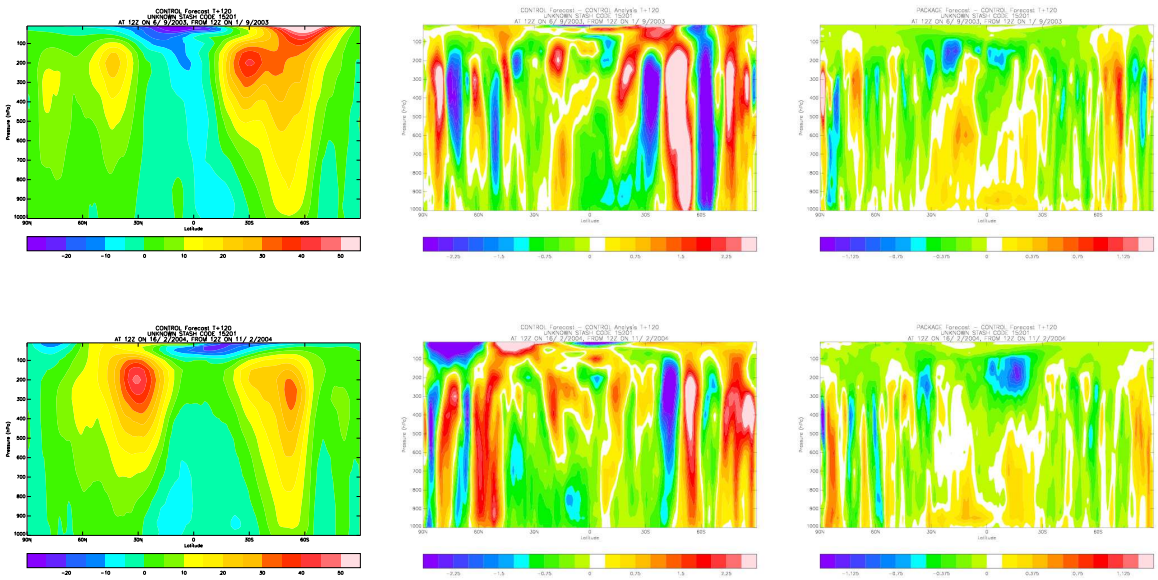

Figure 23: *Impacts on zonally averaged day 5 forecasts of zonal wind. Jul-Sep 2003 (top row) and Dec-Feb 2003/04 (bottom row) case studies. Control forecast (left), control forecast errors (middle), and impact of full package (right). Units are m/s.*

the large changes in convective rainfall over tropical land. Over tropical oceans the convection changes contribute similar reductions in convective rainfall seen with the 8B BL scheme . In the extra-tropics there is an increase in convective rainfall and a small decrease in large scale rainfall. We can also split the contribution from the convection changes into those from the corrections and those from the reduction of CAPE closure adjustment timescale from 1 hour to 30 minutes. The dominant contribution in the tropics comes the reduction in the CAPE closure adjustment timescale. At first sight this seems counter intuitive as a reduction in CAPE timescale should make convection more intense for a given amount of CAPE in the atmosphere. However, tests with the aqua-planet have shown that at shorter CAPE timescales a new equilibrium is reached where there is generally less CAPE available at any given time and convection is therefore less intense. This response is not fully understood and involves a complex interplay between convection, large-scale dynamics and other physical processes. It is also unclear why the response should be so different over land and ocean? One possible hypothesis is that the excessive precipitation over the oceans in the current model is suppressing the precipitation over land via the large-scale divergent circulation (too much descent over land). Reducing the oceanic tropical precipitation may remove this suppression mechanism. This hypothesis was tested by performing a sensitivity test where the CAPE closure is kept at 1 hour over land and only changed to 30 minutes over the ocean (Fig. 29). The results show that this hypothesis of indirect effects only accounts for a small proportion of the total increase in precipitation over land.

5 Trials of the package of changes with full data assimilation.

a NWP index impacts

The impacts on the NWP index from the trials with data assimilation (2-4 above) are shown in table 3.

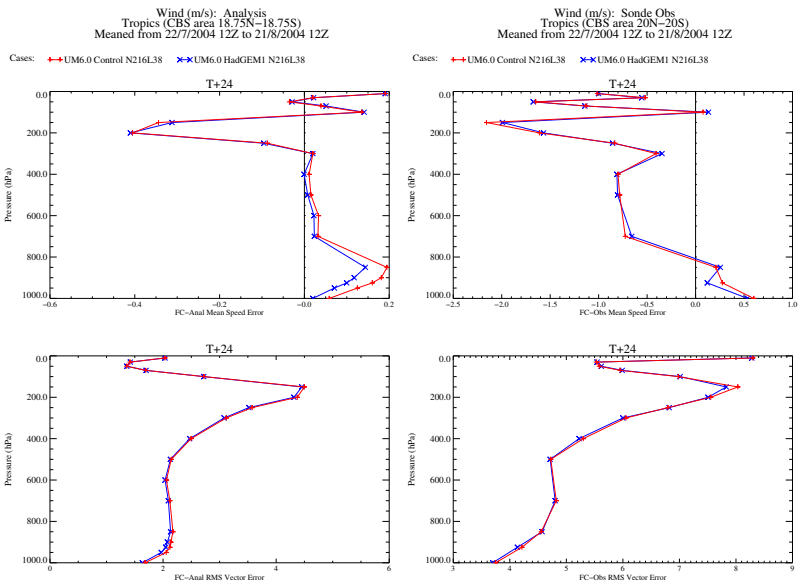

Figure 24: *Objective verification of day 1 winds as a function of height (pressure) from the Jul-Aug 2003 3D-Var trial of the full package. Top row shows the wind speed bias and the bottom row the RMS vector wind errors. The left hand panels are for verification against analyses and the right hand for verification against sondes.*

	vs Analyses	vs Observations
Summer 3D-Var Trial (*without* convection changes)	0.43	-0.14
Summer 3D-Var Trial (*with* convection changes)	0.51	-
Winter 3D-Var trial (only up to 13/1/2005)	2.26	2.19
Winter 4D-Var parallel trial (14/12/2004-6/1/2005)	1.33	1.80

Table 3: *Impact on NWP index 36 month estimate. Positive results imply an improvement in overall skill.*

The winter 4D-Var trial shows an increase of 1.80 (1.33) in the NWP index verifying against observations (analyses). The winter 3D-Var trial shows even larger improvements. For the summer 3D-Var trial the impact on the NWP index is neutral (-0.14) against observations and positive (0.43) against analyses. Inclusion of the convection changes gives a further small improvement. Looking day by day at the scores for summer the majority of cases show improvements but there were 2 or 3 days when the package had increased RMS errors at longer forecast ranges in the extra-tropics. The breakdown of the NWP index into individual components for the Dec-Jan 2004/05 parallel trial (Fig.30) and Jun-Aug 3D-Var trial (Fig.31) show improvements are dominated by the tropical winds at 850hPa and 250 hPa . During Dec-Jan there are also consistent reductions in extra-tropical RMS errors and increases in skill. The exception are geopotential heights in the Southern Hemisphere which are worse. This might be due to increasing the existing mid-tropospheric warm bias in the summer hemispheres (e.g. SH in DJF and NH in JJA).

b Time Series Verification from Parallel Trial.

Finally we present some examples of time series verification from the parallel trial with 4D-Var to show the day by day impacts on objective scores. These clearly show the consistent improvements in verification measures.

- Reduced positive bias in Northern Hemisphere MSLP and reduced RMS errors at T+72 (Fig.32)

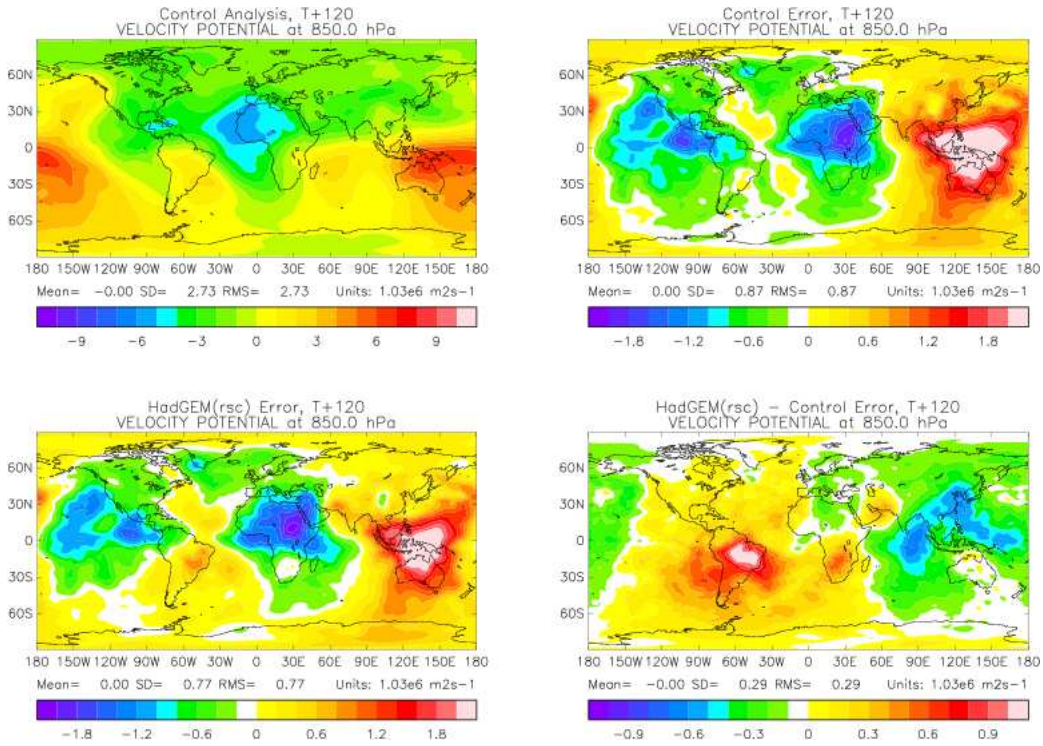

Figure 25: *Velocity potential at 850hPa from the Dec-Jan 2003/04 trial. Control analysis (top left), day 5 control error (forecast - analysis)(top right), day 5 new physics package error (bottom left), day 5 forecast difference (package - control).*

- Reduced negative bias in tropical MSLP and reduced RMS errors at T+72 (Fig.33)
- Improvements to tropical winds at 850hPa in both wind speed bias and RMS vector wind errors (Fig.34).
- Improved 1.5m temperatures at T+24 (Fig.35).

6 Summary and Conclusions.

We have evaluated the 3C large scale precipitation scheme, the 8B BL scheme, increased Saharan albedo, and a change in the CAPE adjustment timescale for convection from 1 hour to 30 minutes. A number of coding errors have also been corrected in the boundary layer and convection parametrizations. These changes bring the global NWP model physical parametrizations in close agreement with those in the climate version, HadGEM1 (with the exception of the 30m CAPE timescale). On balance this package of changes was found to be an improvement and implemented operationally into the global model as cycle G34 on 18th January 2005. In summary, the main impacts of the changes are;

Advantages

- Large improvements(~2 points) in the NWP index for winter (Dec-Feb) and smaller improvements in summer (Jul-Aug).
- Improved tropical circulation and verification statistics
  - Reduced convective precipitation over tropical oceans and increases over tropical land.
  - Reduced RMS errors in tropical winds.

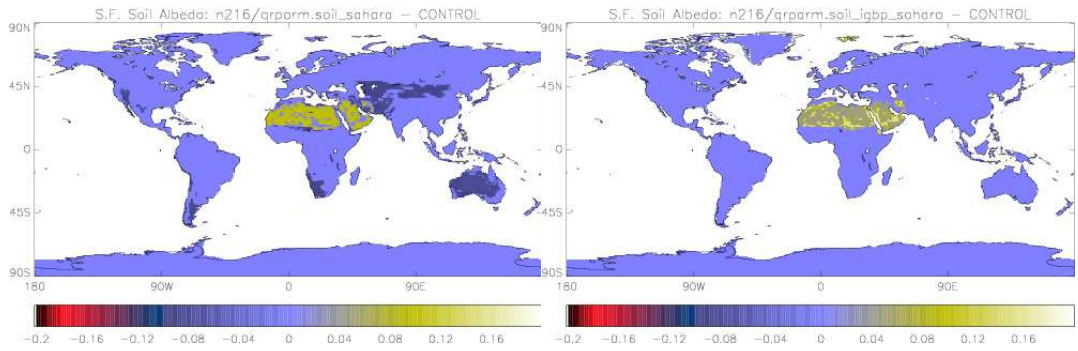

Figure 26: *The increase in Saharan albedo with the Wilson and Henderson-Sellers land use dataset (left panel) and with the IGBP land use dataset (right panel). See text for explanation.*

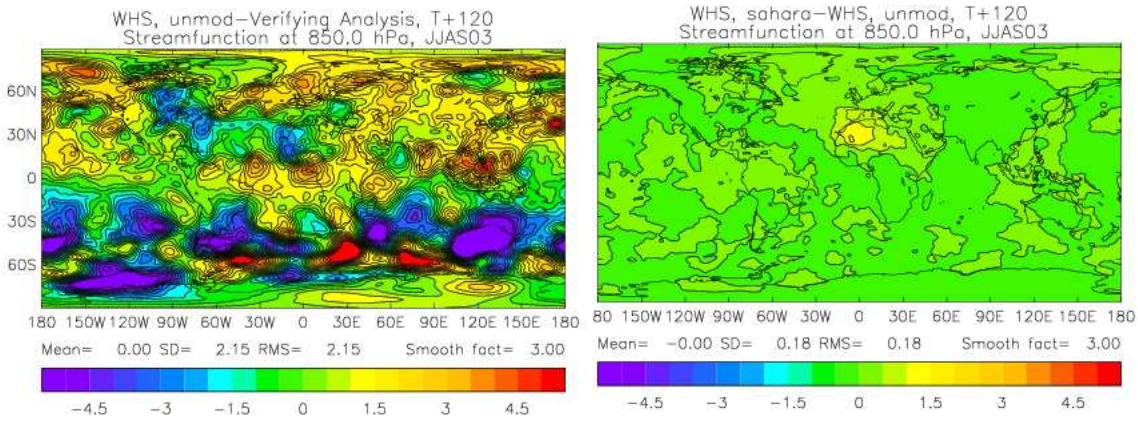

Figure 27: *Impact of Saharan albedo change on 850hPa streamfunction. Left panel shows the stream function error at day 5 in the control experiment and the right panel shows the impact of the Saharan albedo change (experiment-control). The negative error (cyclonic circulation) over the Sahara is reduced with this change.*

  - Reduced warm bias & reduced RMS errors in tropical mid-tropospheric temperatures.
  - Reduced systematic errors in tropical divergent and rotational winds.

- Improved extra-tropical scores (e.g. MSLP), particularly during Dec-Feb.
- Reductions in cloud cover over land, in particular the excessive daytime low cloud cover over Iraq.
- Reduced cloud cover over the subtropical oceans - improved comparisons with GERB planetary albedo over the subtropical Atlantic and with ERBE planetary albedo.
- Improved 1.5m temperatures over extra-tropical land in terms of both bias and RMS error. Largely associated with reductions in cloud.
- Improved surface temperatures, surface & top-of-atmosphere radiative fluxes, sensible heat flux and circulation over the Sahara.

Disadvantages

- Increase to the existing warm bias in the extra-tropics.

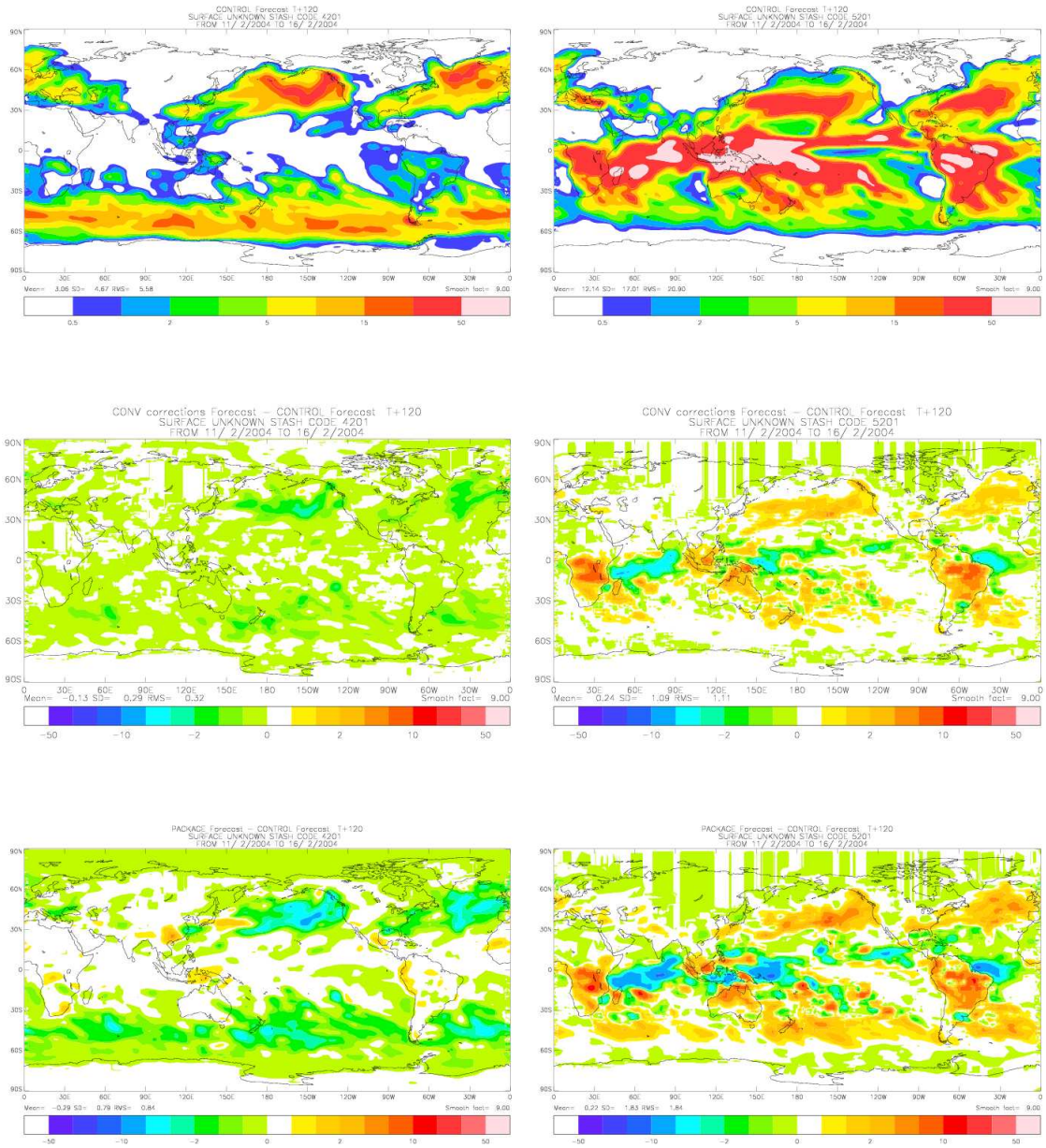

Figure 28: *Impacts on day 5 (accumulated) large-scale (left panels) and convective (right panels) rainfall during Dec-Feb. Control forecast in top row, Impact of ALL convection changes (2nd row), impact of full package (bottom row)*

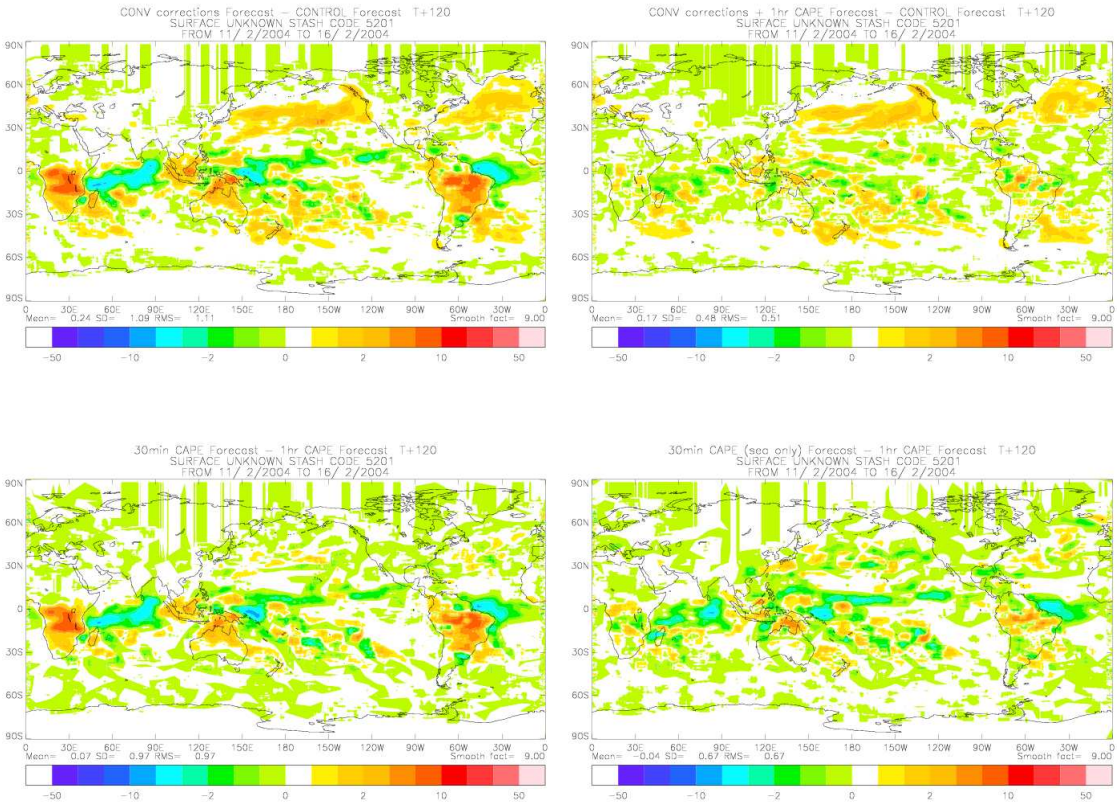

Figure 29: *Impacts on day 5 (accumulated) convective rainfall during Dec-Feb. Impact of ALL changes to convection (top left), impact of convection corrections alone (top right), impact of reducing CAPE closure timescale from 1 hour to 30 minutes (bottom left), and impact of reducing CAPE closure to 30 minutes over the oceans only (bottom right).*

- Increased cold bias at 250hPa in the tropics.
- Possibly less LW and SW cloud forcing in the ITCZ in comparisons with ERBE. This result may be dominated by a particular region as comparisons with GERB in the tropical Atlantic suggested improvements in LW cloud forcing (OLR) due to reduced convective activity.

Other changes

- Increased convective precipitation and reduced large-scale precipitation in the extra-tropical storm tracks. Overall changes to total precipitation in the extra-tropics are small and show both increases and decreases in precipitation.

The changes have had largest beneficial impacts on the tropical circulation and precipitation errors, and on near surface temperatures over land. The tropical circulation appears to improve via a reduction in convective precipitation and diabatic heating over the oceans coming from the 8B BL scheme and the reduced CAPE adjustment timescale. The origin of the reduction in tropical oceanic precipitation from the 8B BL is difficult to diagnose, but one hypothesis is that a reduction in evaporation over the subtropical oceans imply less moisture supply for deep convection in the ITCZ. The reduced evaporation may be linked to increased near surface humidities arising from shallower mixing in the decoupled BL types that have replaced the well mixed BL types. The increase in tropical precipitation over land is also beneficial and comes largely from the reduced CAPE adjustment timescale. Experiments were carried out to try and determine if increased precipitation over tropical land is (i) a direct consequence of the reduction in CAPE adjustment timescale over land or (ii) an indirect effect of the reduced oceanic convection giving less suppression of convection over land via changes in the large-scale divergent circulation. The largest signal came from the direct effect of reducing the CAPE adjustment timescale over land.

The changes to low cloud in the subtropics appear to give improved comparisons with both ERBE and GERB planetary albedo and SW cloud forcing. However, the reductions in LW cloud forcing in the ITCZ are more ambiguous, showing worse results against ERBE averaged over all latitudes, but some evidence of improvements locally in the tropical Atlantic for comparisons with GERB. Reductions of cloud over land also seem to improve near surface temperatures. Over the northern hemisphere in summer the increased net SW radiation at the surface helps reduce a cold bias in the model. In winter the reduced cloud gives reduced downward LW which helps alleviate a warm bias in high latitudes. Surface fluxes and near surface humidities over the oceans are more difficult to evaluate and more diagnostic work is planned to compare the model with available observations (e.g. buoys, ships etc.).

Finally, the increase in Saharan albedo was motivated by comparisons with ERBE and GERB top of the atmosphere clear sky radiative fluxes which suggested surface albedo was underestimated. The increased albedo has improved the top of the atmosphere radiation balance in the model compared to GERB and reduced the excessive sensible heating of the surface.

7 Acknowledgements

Thanks to Paul Selwood & Richard Barnes for providing code optimizations and building UM components, Tim Hewson for developing the new geopotential height diagnostic and Andy Malcolm and Paul Earnshaw for coding and testing. Thanks also to Julian Heming and Paul Earnshaw for running the 3D-Var controls.

References

Allan, R., A. Slingo, S. F. Milton, and I. Culverwell, 2004: Exploitation of geostationary earth radiation budget data using simulations from a numerical weather prediction model: Methodology and data validation. *submitted to J. Geophys. Res.*

Davies, T., M. Cullen, A. Malcolm, M. Mawson, A. Staniforth, A. White, and N. Wood, 2005: A new dynamical core for the met office's global and regional modelling of the atmosphere. *submitted to Q. J. R. Meteorol. Soc*.

Lock, A. P., A. R. Brown, M. R. Bush, G. M. Martin, and R. N. B. Smith, 2000: A new boundary layer mixing scheme. Part I: Scheme description and single-column model tests. *Mon. Wea. Rev.*, **128**(9), 3187–3199.

Lock, A., 2003a: Boundary Layer Processes, Option 6/8A:The parametrization of turbulent fluxes above the surface. Unified Model Documentation Paper 24, Available from The Met Office.

——, 2003b: Boundary Layer Processes, Option 6/8B:Revisions to the 6/8A parametrization of turbulent fluxes above the surface. Unified Model Documentation Paper 24, Available from The Met Office.

Martin, G. M., M. R. Bush, A. R. Brown, A. P. Lock, and R. N. S. Smith, 2000: A new boundary layer mixing scheme. Part II: Tests in climate and mesoscale models. *Mon. Wea. Rev.*, **128**, 3200–3217.

Neale, R., and J. Slingo, 2003: The maritime continent and its role in the global climate : A gcm study. *J. Climate*, **116**, 834–848.

Webb, M., C. A. Senior, S. Bony, and J. Morcrette, 2001: Combining ERBE and ISCCP data to assess clouds in the Hadley Centre, ECMWF and LMD atmospheric climate models. *Clim. Dyn.*, **17**, 905–922.

Wilson, D. R., and S. P. Ballard, 1999: A microphysically based precipitation scheme for the U.K. Meteorological Office Unified Model. *Q. J. R. Meteorol. Soc.*, **125**, 1607–1636.

Wilson, D., and R. Forbes., 2004: The large scale precipitation parametrization scheme. Unified Model Documentation Paper 26, Available from The Met Office, Fitzroy Rd, Exeter, Devon, EX1 3PB, UK.

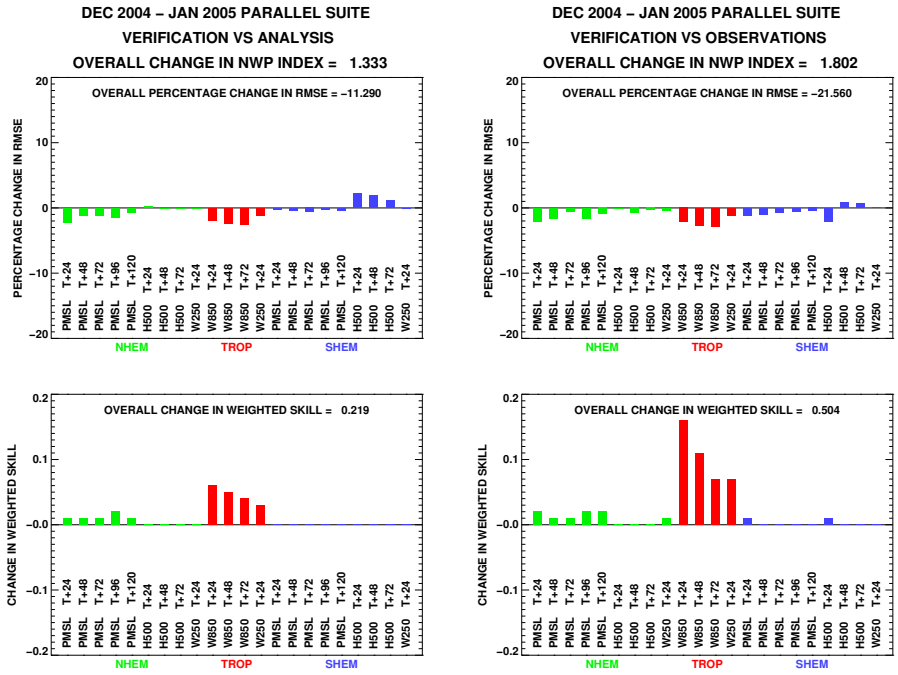

Figure 30: *Impact on NWP index components from Dec 2004-Jan 2005 Parallel trial. Top panels show the change in RMS error and bottom panels the change in skill. The left figure is for verification against analyses and the right for verification against observations. The period covered is 24 days from 12UTC 14/12/2004 to 12UTC 6/1/2005.*

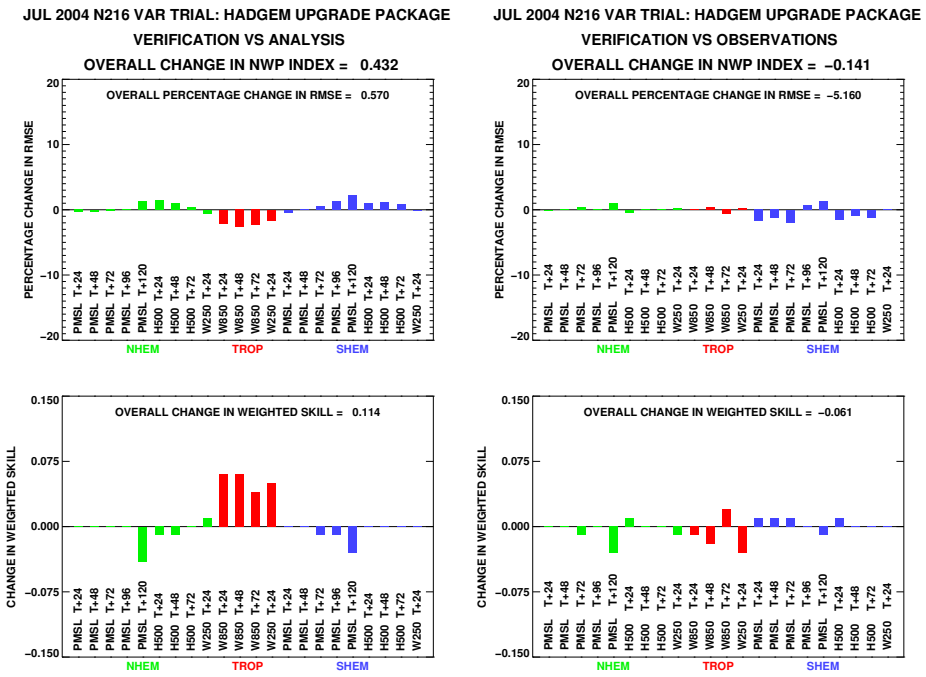

Figure 31: *As figure 30 but for the Jul-Aug 2003 3D-Var parallel trial (**without** convection changes).*

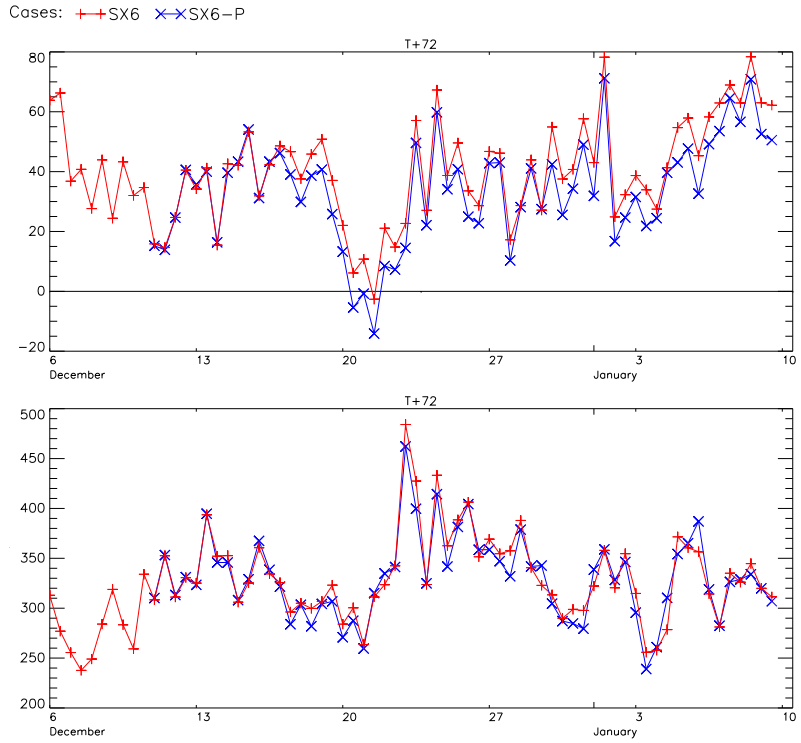

Figure 32: *Time series verification for day 3 NH MSLP from Dec 2004-Jan 2005 parallel trial. Mean Error (top) and RMS error (bottom). Units are Pa. Verification against analyses.*

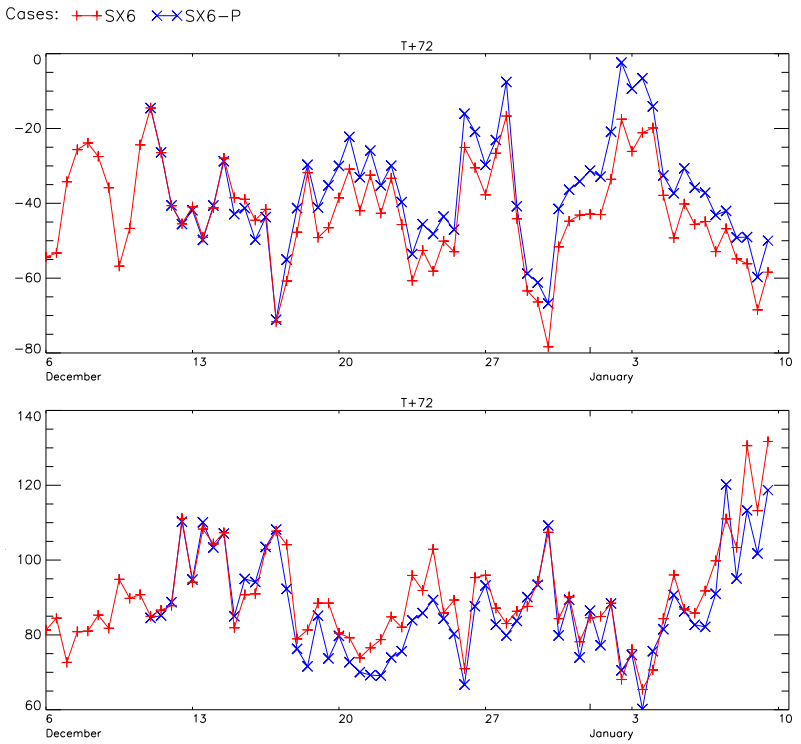

Figure 33: *As fig 32 but for day 3 Tropical MSLP . Verification against analyses.*

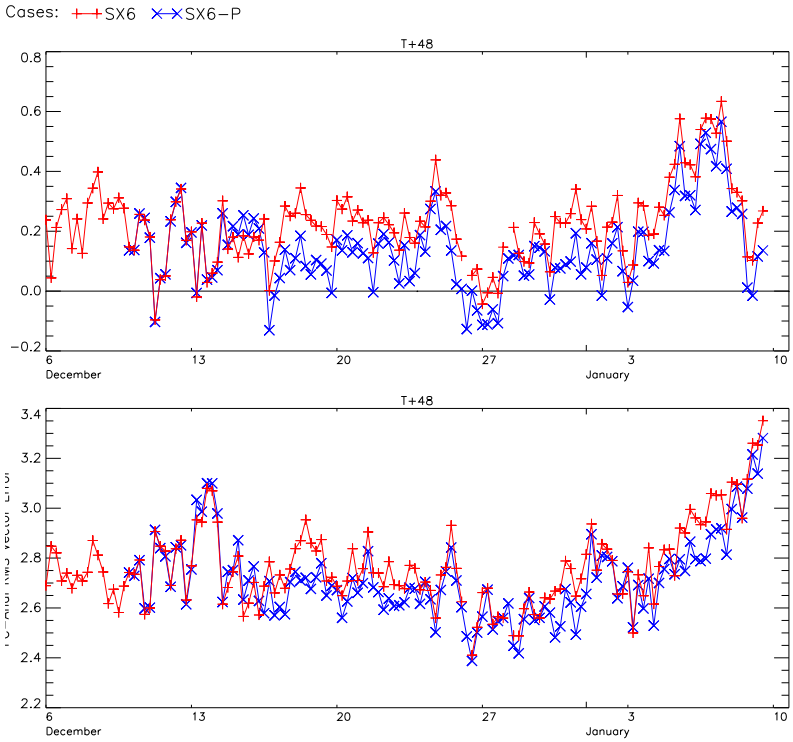

Figure 34: *Time series verification for day 2 Tropical winds @ 850hPa from Dec2004-Jan 2005 parallel trial. Mean wind speed error (top) and RMS vector wind error (bottom). Units are m/s. Verification against analyses.*

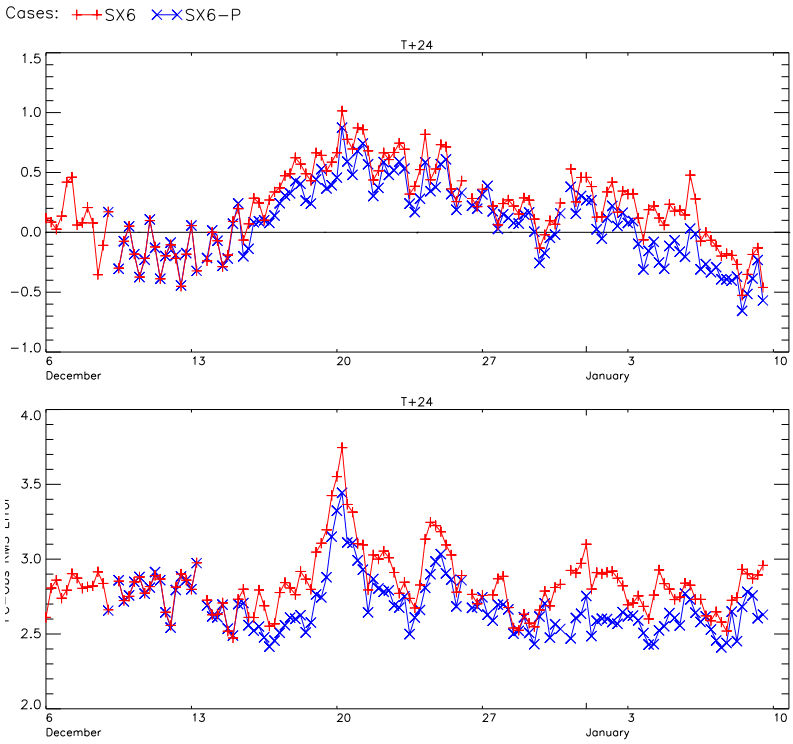

Figure 35: *Time series verification for T+24 1.5m temperatures from Dec2004-Jan 2005 parallel trial. Mean Error (top) and RMS error (bottom). Units are K. Verification is against SYNOPS.*